Article

Molecular Cell

Sterol Oxidation Mediates Stress-Responsive Vms1 Translocation to Mitochondria

Graphical Abstract

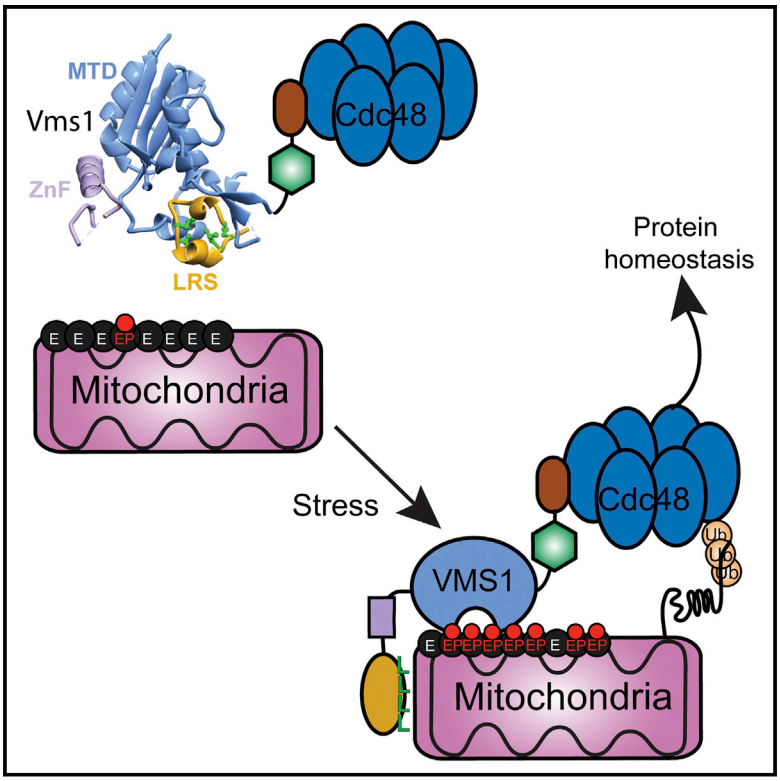

Authors

Jason R. Nielson, Eric K. Fredrickson, T. Cameron Waller, ..., Zhenjian Lin, Christopher P. Hill, Jared Rutter

Correspondence

hill@biochem.utah.edu (C.P.H.), rutter@biochem.utah.edu (J.R.)

In Brief

Vms1 translocates to damaged mitochondria in response to stress by unknown mechanisms. Here, Nielson et al. demonstrate that Vms1 mitochondrial translocation is regulated by a hydrophobic intramolecular interaction and the accumulation of an oxidized sterol, ergosterol peroxide. This study implicates sterol oxidation as a mechanism for mitochondrial stress response.

Highlights

- Stress induces Vms1 mitochondrial localization independently of protein interaction
- Ergosterol peroxide (EP) binding mediates Vms1 mitochondrial localization
- The Vms1 leucine-rich sequence (LRS) binds the mitochondrial targeting domain (MTD)
- The LRS competes with EP for MTD binding to inhibit Vms1 mitochondrial localization

Nielson et al., 2017, Molecular Cell *68*, 673–685
November 16, 2017
https://doi.org/10.1016/j.molcel.2017.10.022

Molecular Cell
Article

Sterol Oxidation Mediates Stress-Responsive Vms1 Translocation to Mitochondria

Jason R. Nielson,[1,4] Eric K. Fredrickson,[1,4] T. Cameron Waller,[1] Olga Zurita Rendón,[1,2] Heidi L. Schubert,[1] Zhenjian Lin,[3] Christopher P. Hill,[1,*] and Jared Rutter[1,2,5,*]
[1]Department of Biochemistry
[2]Howard Hughes Medical Institute
University of Utah School of Medicine, Salt Lake City, UT 84112, USA
[3]Department of Medicinal Chemistry, University of Utah College of Pharmacy, Salt Lake City, UT 84112, USA
[4]These authors contributed equally
[5]Lead Contact
*Correspondence: hill@biochem.utah.edu (C.P.H.), rutter@biochem.utah.edu (J.R.)
https://doi.org/10.1016/j.molcel.2017.10.022

SUMMARY

Vms1 translocates to damaged mitochondria in response to stress, whereupon its binding partner, Cdc48, contributes to mitochondrial protein homeostasis. Mitochondrial targeting of Vms1 is mediated by its conserved mitochondrial targeting domain (MTD), which, in unstressed conditions, is inhibited by intramolecular binding to the Vms1 leucine-rich sequence (LRS). Here, we report a 2.7 Å crystal structure of Vms1 that reveals that the LRS lies in a hydrophobic groove in the autoinhibited MTD. We also demonstrate that the oxidized sterol, ergosterol peroxide, is necessary and sufficient for Vms1 localization to mitochondria, through binding the MTD in an interaction that is competitive with binding to the LRS. These data support a model in which stressed mitochondria generate an oxidized sterol receptor that recruits Vms1 to support mitochondrial protein homeostasis.

INTRODUCTION

Many critical cellular activities depend on mitochondria, including bioenergetics, biosynthesis, and signaling (Calvo and Mootha, 2010). Therefore, it is not surprising that mitochondrial dysfunction is a hallmark of a wide variety of diseases and disorders, including neurodegeneration and heart disease (Lin and Beal, 2006). Major effectors of mitochondrial dysfunction are the reactive oxygen species (ROS) that result from inefficiencies in the electron transport chain (Circu and Aw, 2010) and can lead to DNA damage, protein misfolding and aggregation, altered membrane permeability, disturbed Ca^{2+} homeostasis, disrupted oxidative phosphorylation, and, eventually, cell death (Zorov et al., 2014).

To combat these deleterious outcomes and maintain mitochondrial function and integrity, cells use a network of mitochondrial quality control systems. One of these is the ubiquitin-proteasome system (UPS), which can remove and degrade proteins from the mitochondrial outer membrane (MOM). Ubiquitylated MOM proteins, such as the mitofusins (e.g., Mfn1 and Mfn2) (Tanaka et al., 2010) and TOM complex subunits (e.g., Tom40 and Tom70) (Yoshii et al., 2011), are extracted by the AAA-ATPase p97/VCP (Livnat-Levanon and Glickman, 2011) and targeted for degradation by the cytoplasmic 26S proteasome (Heo and Rutter, 2011).

Previously, we showed that cytoplasmic Vms1 (VCP/Cdc48-associated mitochondrial stress-responsive 1) serves as an adaptor to promote the mitochondrial localization of Cdc48, the *S. cerevisiae* p97 homolog, and its cofactor Npl4 when cells are exposed to mitochondrial stressors such as antimycin, oligomycin, and H_2O_2 (Heo et al., 2010), as well as paraquat and DMNQ (unpublished data). In the absence of the Vms1-Cdc48 complex, cells accumulate ubiquitylated mitochondrial proteins, suffer progressive mitochondrial failure, have elevated levels of mitophagy, and fail to survive under mitochondrial stress conditions (Heo et al., 2010).

Vms1 translocation from the cytosol to mitochondria under conditions of mitochondrial stress requires its highly conserved mitochondrial targeting domain ($Vms1^{MTD}$) (Heo et al., 2013). $Vms1^{MTD}$ localization to mitochondria in unstressed conditions is prevented by an intramolecular interaction with the Vms1 N-terminal leucine-rich sequence ($Vms1^{LRS}$). In the absence of the $Vms1^{LRS}$, $Vms1^{MTD}$ constitutively localizes to mitochondria in the presence or absence of stress (Heo et al., 2013), suggesting that translocation of the full-length protein is regulated by this intramolecular interaction. Localization is also regulated by mitochondrial damage because full-length wild-type Vms1 localizes to damaged, but not undamaged, mitochondria, indicating that damaged mitochondria are specifically marked for Vms1 recruitment (Heo et al., 2013).

These data prompt several questions: First, how does the $Vms1^{LRS}$ inhibit localization of the $Vms1^{MTD}$ to mitochondria? Second, what is (are) the mitochondrial molecule(s) that mediate $Vms1^{MTD}$ binding to mitochondria? Third, what is the stress signal that modifies mitochondria and/or Vms1 to promote Vms1 translocation to damaged mitochondria? Herein, we describe a mechanism whereby Vms1 localization to mitochondria results from interaction with the stress-induced oxidized sterol ergosterol peroxide, the binding of which is opposed by the intramolecular Vms1 LRS-MTD association.

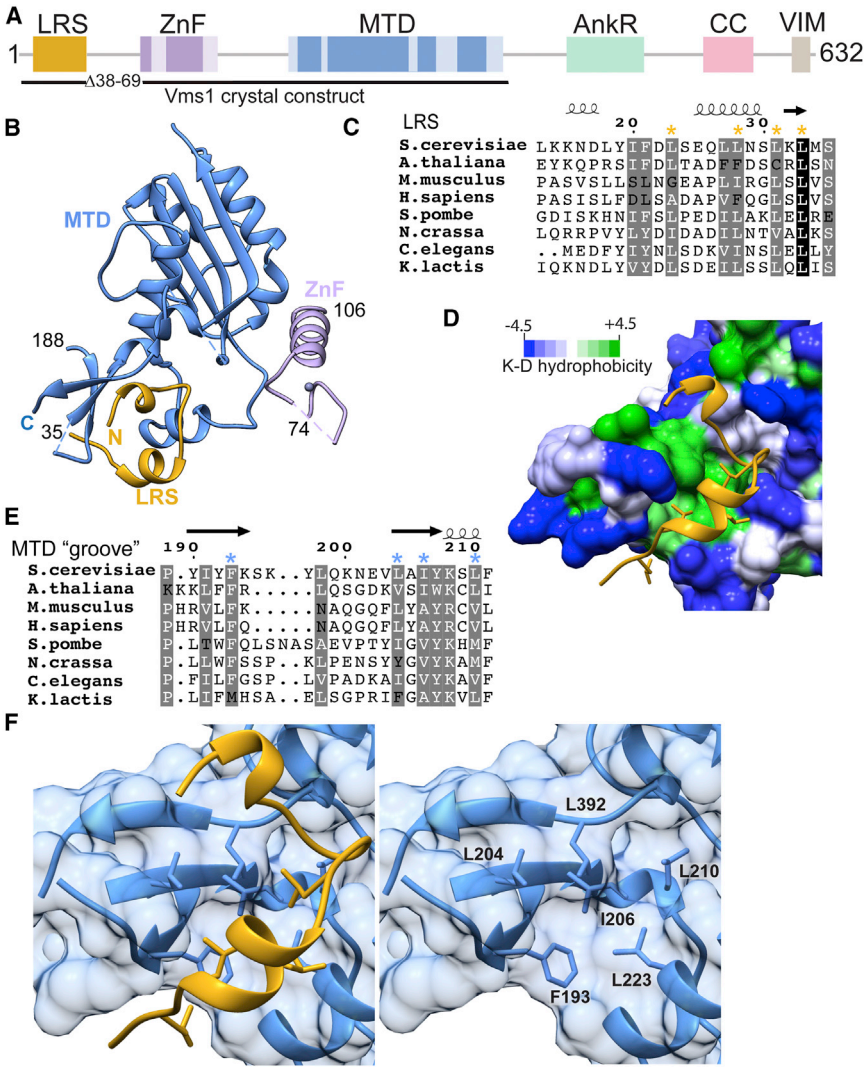

Figure 1. Structure of Vms1 Region that Regulates Mitochondrial Localization

(A) Schematic representation of the domain structure of Vms1. Black line below indicates the crystallized construct. LRS, leucine-rich sequence; ZnF, zinc finger; MTD, mitochondrial targeting domain; AnkR, ankryin repeat; CC, coil-coil; VIM, VCP-interacting motif. Grayed out areas, including all segments between domains, denote regions not visible in the electron density maps.

(B) Vms1$^{LRS\text{-}ZnF\text{-}MTD}$ ribbon representation. The Zn ion is represented by a gray sphere. Dashed lines indicate residues not visible in the structure, except for the large segments 36–73 and 107–187, the ends of which are labeled with residue numbers.

(C) Alignment of LRS residues visible in (B). White letters with gray background indicates similarity. White letters with a black background indicates identity. Yellow asterisks indicate Leu residues whose mutation abolished MTD interaction (Heo et al., 2013).

(D) LRS Leu 23, 28, 31, and 33 (yellow), the same residues marked by asterisks in (C), are shown explicitly on the Vms1 ribbon representation. The MTD is shown as a surface representation, colored by Kyte-Doolittle (K-D) hydrophobicity (Kyte and Doolittle, 1982).

(E) Alignment of MTD hydrophobic groove that contacts the LRS. Conservation is colored as in (C). Blue asterisks indicate residues shown in (F).

(F) Ribbon representation showing the interaction between the MTD and LRS on the left. Side chains are shown for hydrophobic residues in each domain that are buried at the LRS-MTD interface. The LRS is removed on the right to better visualize the MTD residues.

See also Figure S1.

RESULTS

Vms1 Crystal Structure Shows the LRS Binding a Hydrophobic Groove on the MTD Surface

To further understand the intramolecular regulation of Vms1 localization to mitochondria, we visualized the Vms1 LRS-MTD interaction by determining a crystal structure of Vms1$^{LRS\text{-}ZnF\text{-}MTD}$ (Figure 1A). Many constructs of *S. cerevisiae* Vms1 were prepared by expression and purification from *E. coli* and subjected to crystallization trials. The crystalized construct comprised residues 1–417 and lacked residues 38–69, which are poorly conserved and were predicted to form an unstructured loop (Figure 1A). Removal of this loop had no effect on Vms1 function *in vivo* (Figure S1). The structure was determined using single-wavelength anomalous diffraction from the selenomethionine-substituted protein and was refined at a resolution of 2.7 Å to R_{work}/R_{free} values of 18.7%/24.5% (Table 1).

The Vms1 model comprises the LRS (residues 13–35), portions of the ZnF domain including the Zn^{2+} ion and its coordinating residues (residues 74–80 and 90–106), and the majority of the MTD (residues 188–197, 203–257, 267–286, and 318–397) (Figure 1B). No other residues in the Vms1$^{LRS\text{-}ZnF\text{-}MTD}$ construct are visible in the crystal structure, presumably because they are highly mobile or because they were excised by the low level of protease that we found to be necessary to grow crystals (Figure 1A). The Vms1^{MTD} adopts a fold in which a mixed β sheet is flanked on both sides by α helices (Figure 1B). Comparison with structures in the PDB by the DALI server (Holm and Rosenström, 2010) indicated that the MTD fold is most closely related to eukaryotic peptide chain release factor subunit 1 (3e1y-C), although the overlap is only on 117 pairs of Cα atoms and gives a large root-mean-square deviation (5.7 Å).

LRS and MTD Mutations that Disrupt the LRS-MTD Interface Alter Mitochondrial Localization

The LRS (residues 13–35) packs against the MTD through an interface that includes LRS residues that are hydrophobic and conserved. The N-terminal helix (residues 14–18) is not highly conserved (Figure 1C). Conserved hydrophobic residues

Table 1. Crystallographic Data Collection and Refinement

Data Collection and Refinement	$Vms1^{LRS\text{-}ZnF\text{-}MTD}$
Data Collection	
Beamline	SSRL 11-1
Space group	$P3_221$
Cell dimensions: a, b, c (Å)	62.84, 62.84, 154.32
Resolution (Å)	24–2.7 (2.8–2.7)
I/σI	33.6 (2.0)
Completeness (%)	99.8 (98.3)
R_{pim}[a] (%)	2.0 (39.0)
Redundancy	10.3 (9.1)
CC1/2[b]	(0.793)
Refinement	
Resolution (Å)	24–2.7 (2.76–2.7)
Number of reflections	10,250
R_{work}[c]/R_{free}[d] (%)	18.7 (30.5)/24.5 (35.9)
Number of protein atoms	1,746
Number of water molecules	29
Number of ligands	1
RMSD: bond lengths (Å)/angles (°)	0.007/0.95
B factors: protein ($Å^2$)	107.0
B factors: zinc ($Å^2$)	127
B factors: solvent ($Å^2$)	96.3
Φ/Ψ: most favored/allowed (%)	92.4/7.1

Values in parentheses refer to the highest resolution shell.

[a] $R_{pim} = \sum_{hkl}\left[\frac{1}{N-1}\right]^{\frac{1}{2}}\sum_i |I_i(hkl) - \overline{I(hkl)}| / \sum_{hkl}\sum_i I_i(hkl)$ (Weiss, 2001)

[b] $CC = \sum(x-(x))(y-(y))/[\sum(x-(x))^2\sum(y-(y))^2]^{1/2}$

[c] $R_{work} = \Sigma||F_o| - |F_c||/\Sigma|F_o|$, where $|F_o|$ and $|F_c|$ are the observed and calculated structure factor amplitudes, respectively, summed over structure factors used in refinement calculations

[d] R_{free} = R factor calculated using a random set of reflections (5% of total) that were not used in refinement calculations

follow in an extended turn (residues 19–24) that are buried against the MTD (Figure 1C; Ile20, Phe21, and Leu23). This is followed by a second helix (residues 25–30) that includes two conserved Leu residues that are partially buried. Lastly, residues 31–35 constitute a short loop containing highly conserved and buried Leu residues (Figure 1C; Leu31 and Leu33). The only residue in the entire LRS that is conserved and not buried is Ser35. We previously identified the conserved Leu residues (Leu23, Leu28, Leu31, and Leu33) in the LRS as being important for the interaction with the MTD (Heo et al., 2013) (Figure 1C). Our structure revealed that these residues mediate multiple hydrophobic inter-domain contacts at the LRS-MTD interface (Figure 1D). Moreover, mutation of these LRS Leu residues led to greater mitochondrial localization of Vms1 (Heo et al., 2013), which suggests that displacement of the LRS may unmask a surface of Vms1 that is important for binding to a mitochondrial receptor and/or the mitochondrial membrane.

The MTD surface buried by the LRS is a large (1,205 $Å^2$) groove that is predominately composed of hydrophobic residues that contact the conserved LRS hydrophobic residues (Figure 1D). The majority of these hydrophobic MTD residues reside in two strands (residues 190–194 and 203–207), although Leu210, Leu223, and Leu392 also contribute (Figures 1E and 1F). A few hydrophilic residues, which are not conserved, also lie at the LRS/MTD interface (Asn227, His253, and Arg255).

Guided by the structure, we further explored the importance of residues at the LRS-MTD interface and across the MTD surface for mitochondrial localization by determining the localization of Vms1-GFP in *S. cerevisiae* when 19 conserved MTD residues were substituted individually or in clusters. Localization was tested in the context of the $Vms1^{MTD}$-GFP construct because its constitutive and robust mitochondrial localization simplifies a quantitative comparison between mutants. We identified several mutants that displayed impaired mitochondrial localization of the $Vms1^{MTD}$-GFP fusion protein and others that did not (representative examples are shown in Figures 2A and 2B; a summary is shown in Figures 2D and 2E). The reduction in mitochondrial localization did not result from a reduction in protein abundance because the abundance of each mutant is similar to that of wild-type (Figure 2C).

Building on the earlier mutational study of conserved LRS Leu residues (Heo et al., 2013), we verified that the MTD residues that are located at the LRS-MTD interface are also important for LRS-MTD binding in solution. This was done by mutating the MTD residues Phe193 or Ile204, which are buried against the LRS (Figures 2D and 2E). In both cases, co-expression of these mutated MTD-GFP constructs with an LRS-hemagglutinin (HA) construct showed impaired interaction in co-immunoprecipitation experiments (Figure 2F). Interestingly, these mutants exhibited reduced mitochondrial localization (Figures 2A and 2B). This is in contrast to the analogous mutations of hydrophobic residues on the LRS side of the interface, which also showed reduced LRS-MTD interaction but displayed increased mitochondrial localization (Heo et al., 2013). These observations are consistent with the model that the LRS masks MTD residues that are important for mitochondrial localization, so that mutation of LRS residues that disrupt the MTD interaction uncovers a surface that promotes mitochondrial localization, whereas mutation of MTD residues that disrupt the LRS interaction might also disrupt a part of the MTD surface that mediates mitochondrial localization.

MTD Surface Residues Close to the LRS Are Also Important for Mitochondrial Localization

Our survey of residues across the MTD surface revealed a number of mutants that are not buried at the LRS interface yet displayed >10% reduced mitochondrial localization (Figures 2C and 2D). These residues were all from the region surrounding the $Vms1^{LRS}$ interaction interface, whereas mutations elsewhere had little or no effect on Vms1 localization (Figures 2A and 2B). For example, Y190D and K194D/K196D, which are within 10 Å of the LRS but are not at the LRS interface and display normal interaction with the $Vms1^{LRS}$, showed >10% reduced localization to mitochondria (Figures 2A, 2B, and 2F). The observation that MTD residues both at and surrounding the LRS interface mediate MTD localization to mitochondria suggests that the localization of Vms1 to mitochondria involves remodeling of

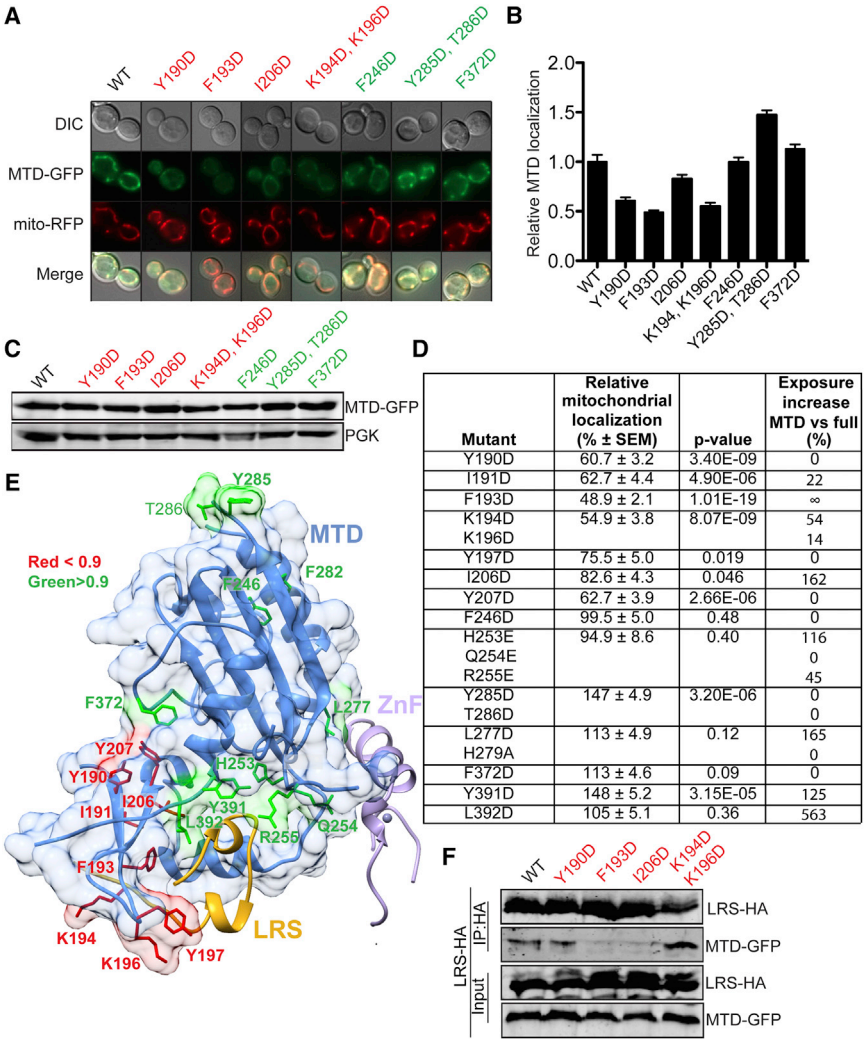

Mutant	Relative mitochondrial localization (% ± SEM)	p-value	Exposure increase MTD vs full (%)
Y190D	60.7 ± 3.2	3.40E-09	0
I191D	62.7 ± 4.4	4.90E-06	22
F193D	48.9 ± 2.1	1.01E-19	∞
K194D	54.9 ± 3.8	8.07E-09	54
K196D			14
Y197D	75.5 ± 5.0	0.019	0
I206D	82.6 ± 4.3	0.046	162
Y207D	62.7 ± 3.9	2.66E-06	0
F246D	99.5 ± 5.0	0.48	0
H253E	94.9 ± 8.6	0.40	116
Q254E			0
R255E			45
Y285D	147 ± 4.9	3.20E-06	0
T286D			0
L277D	113 ± 4.9	0.12	165
H279A			0
F372D	113 ± 4.6	0.09	0
Y391D	148 ± 5.2	3.15E-05	125
L392D	105 ± 5.1	0.36	563

Figure 2. MTD Surface Surrounding the Vms1$^{LRS-MTD}$ Interface Mediates Localization to Mitochondria

(A) *vms1Δ* cells expressing the indicated Vms1^{MTD}-GFP construct and mitochondria-targeted red fluorescent protein (RFP) were grown to mid-log phase and analyzed by fluorescence microscopy. Representative images are shown. DIC, differential interference contrast.

(B) The mitochondrial MTD-GFP intensity from (A) was quantified as described for 100+ cells in each strain over multiple days of imaging. Error bars, mean ± SEM.

(C) Cells from (A) were lysed as described and analyzed by western blot.

(D) Table of MTD residues mutated, with quantified mitochondrial localizations relative to wild-type (WT) (% ± SEM) and p values indicated. Residues were initially mutated in pairs or triplets and only made as single mutants if there was a greater than 10% reduction in MTD localization. Some mutants enhanced mitochondrial localization, indicated by values greater than 1. The far-right column gives the percent increase in relative Å^2 surface exposure of each amino acid in the MTD alone versus the LRS-MTD complex, based on assuming no conformational change upon removing the LRS from the crystal structure.

(E) Ribbon/surface overview of Vms1^{MTD} with mutated residues highlighted. Residues whose mutation exhibited >10% reduction (red) and ≤10% reduction (green) in MTD localization are indicated.

(F) The *vms1Δ* strain was transformed with Vms1$^{1-182}$-HA and the indicated Vms1^{MTD}-GFP construct. Strain lysates were immunoprecipitated with anti-HA antibody. Western blots were performed with anti-HA and GFP antibodies.

the structure to displace the LRS and form a mitochondrial binding surface formed by multiple MTD residues that are either surface exposed or buried at the LRS interface in the Vms1 crystal structure.

Vms1 Binds Mitochondria via a Lipid Species

To better understand how the stress-responsive translocation of Vms1 to mitochondria is regulated, we sought to identify the molecule(s) to which the Vms1^{MTD} binds on the MOM. We initially hypothesized that Vms1 mitochondrial binding is mediated by a protein, and we screened for a reduction of Vms1^{MTD} localization in over 500 genetic mutants, each lacking a unique gene encoding a non-essential, nuclear-encoded mitochondrial protein (Giaever et al., 2002). None of the mutant strains displayed a substantial reduction of Vms1^{MTD} localization to mitochondria (data not shown). Recognizing that Npl4 and other Cdc48 adaptor proteins bind ubiquitin to recruit Cdc48 to ubiquitylated substrates (Schuberth et al., 2004; Ye et al., 2003), we hypothesized that Vms1 might also bind (poly)ubiquitin at the mitochondrial surface. However, we observed that treating mitochondria with the Usp2 deubiquitylating enzyme had no effect on Vms1 interaction with mitochondria (data not shown).

To determine whether any mitochondrial surface protein is required for Vms1 binding, we treated purified mitochondria with Proteinase K. After digestion, we observed efficient degradation of cytosol-exposed mitochondrial proteins (e.g., Tom22 and Fzo1) but very little cleavage of MOM-imbedded (e.g., Por1) and intra-mitochondrial proteins (e.g., Sdh1, Sdh2, and Mia40), suggesting that mitochondrial surface protein had been thoroughly digested without compromising mitochondrial integrity (Figure 3A). Surprisingly, we observed no significant difference in Vms1 affinity toward mitochondria after Proteinase K treatment (Figures 3B and 3C). Although we cannot rule out the possibility that Proteinase K-resistant proteins or loops contribute to Vms1 binding, these results suggested that mitochondrial surface proteins are dispensable for Vms1 binding to mitochondria.

Because MOM protein appears to be dispensable for Vms1 binding, we hypothesized that Vms1 binds mitochondrial lipids. The majority of mitochondrial lipids are phospholipids, with much smaller quantities of sphingolipids and sterols principally

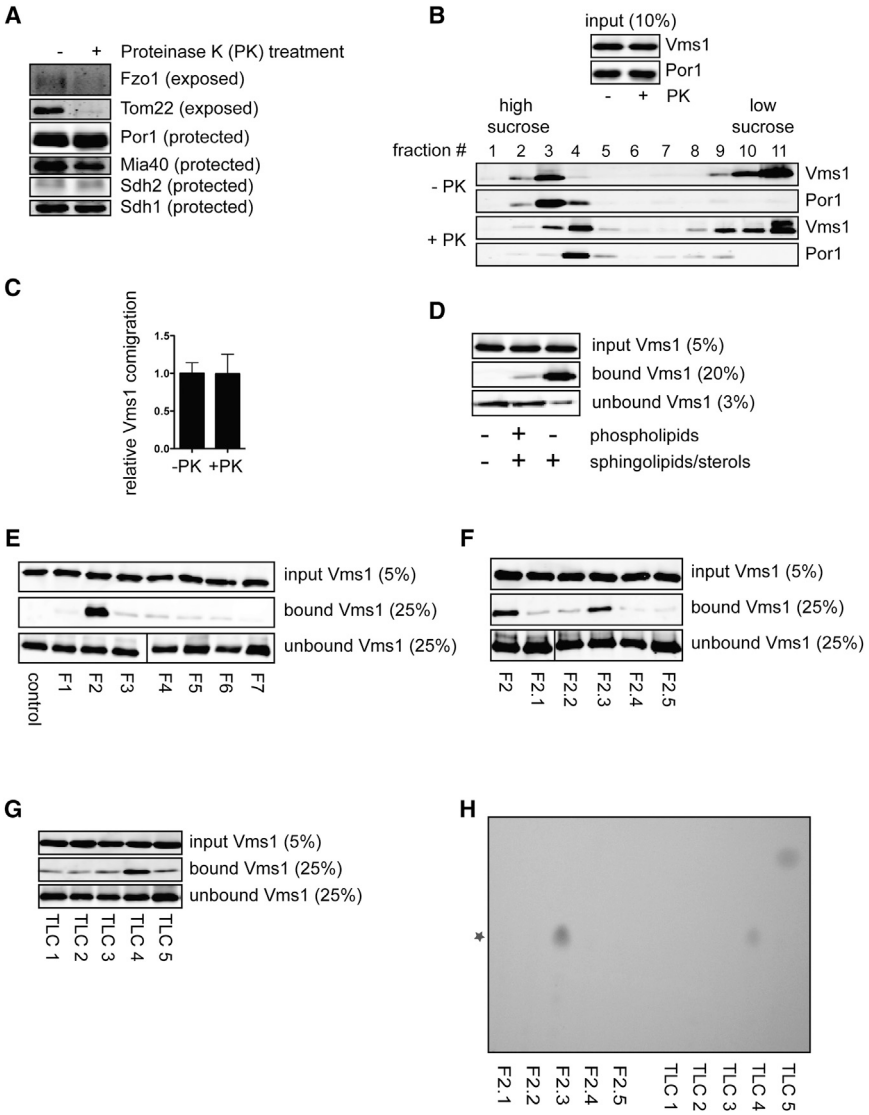

Figure 3. Vms1 Binds a Lipid with Molecular Formula $C_{28}H_{44}O_3$

(A) Purified mitochondria treated with or without Proteinase K were subjected to western blot (20 μg loaded).

(B) Purified Vms1 and untreated or Proteinase K-treated mitochondria were mixed and subjected to sucrose gradient centrifugation. Fractions were collected and subjected to western blot.

(C) Co-migration of Vms1 and Porin from (B) was quantitated over at least 5 experiments in each condition (mean ± SEM).

(D) Floatation assay results for control liposomes and liposomes supplemented with mitochondrial lipids. For liposomes containing mitochondrial lipids, we added lipids isolated from 1 mg mitochondria (determined by measuring protein concentration) per 100 μL liposomes. Purified mitochondrial lipids were added either without modification or following akaline-treatment to generate alkaline-resistant mitochondrial lipids.

(E) Floatation assay results obtained with liposomes prepared with ultra-performance liquid chromatography (UPLC) fractions of purified mitochondrial lipids (lipids from 2 mg mitochondria per 100 μL liposomes).

(F) Fraction 2 in (E) was sub-fractionated, and resulting lipid fractions were incorporated into liposomes (lipids from 1 mg mitochondria per 100 μL liposomes) and subjected to a floatation assay.

(G) Mitochondrial alkaline-resistant lipids were separated into five fractions by TLC. Lipids isolated from each fraction were incorporated into liposomes (lipids from 1 mg mitochondria per 100 μL liposomes) and subjected to a floatation assay.

(H) Lipids from the five UPLC sub-fractions (F) and the five TLC fractions (G) were analyzed by TLC and orcinol stain. The star indicates the common species with formula $C_{28}H_{44}O_3$.

constituting the remainder. Recent studies have described unique roles for both phospholipids (Chu et al., 2013) and sphingolipids (Huang et al., 2012) in recruiting components of the mitophagy machinery to mitochondria. Due to their reactive phosphodiester linkage, phospholipids are susceptible to hydrolysis by mild base, whereas sphingolipids and sterols are not (Guan et al., 2010). We took advantage of this property to create liposomes containing total mitochondrial lipids or liposomes containing a lipid extract that lacked phospholipids. Vms1 bound liposomes containing total mitochondrial lipids, and this binding was enhanced with lipid extract that lacked phospholipids (Figure 3D). The increased level of binding seen upon hydrolysis and removal of the more abundant phospholipids may result from increased local concentration and liposome incorporation of sterols/sphingolipids. These observations indicate that Vms1 binds a sterol or sphingolipid species.

To identify which specific lipid was responsible for Vms1 binding to mitochondria, we assayed for Vms1 binding to high-performance liquid chromatography (HPLC) and thin-layer chromatography (TLC)-fractionated, alkaline-resistant mitochondrial lipids. Sequential, orthogonal fractionation enabled the isolation of two lipid mixtures with highly enriched Vms1 binding activity (Figures 3E–3G). We used TLC to compare lipids found in the two purified fractions that displayed the strongest binding activity toward Vms1, and we identified a single lipid species that was specifically enriched in both fractions (Figure 3H). In parallel, analysis of these binding and adjacent non-binding fractions by liquid chromatography-mass spectrometry (LC-MS) identified a single specific candidate species with a mass corresponding to the molecular formula $C_{28}H_{44}O_3$.

Ergosterol Peroxide Is Necessary and Sufficient for Vms1 Localization to Mitochondria

The molecular formula $C_{28}H_{44}O_3$ corresponds to hundreds of lipid species. To determine the molecular structure of the Vms1-binding lipid, we used silica gel column chromatography to purify a large quantity of the lipid, which we subjected to

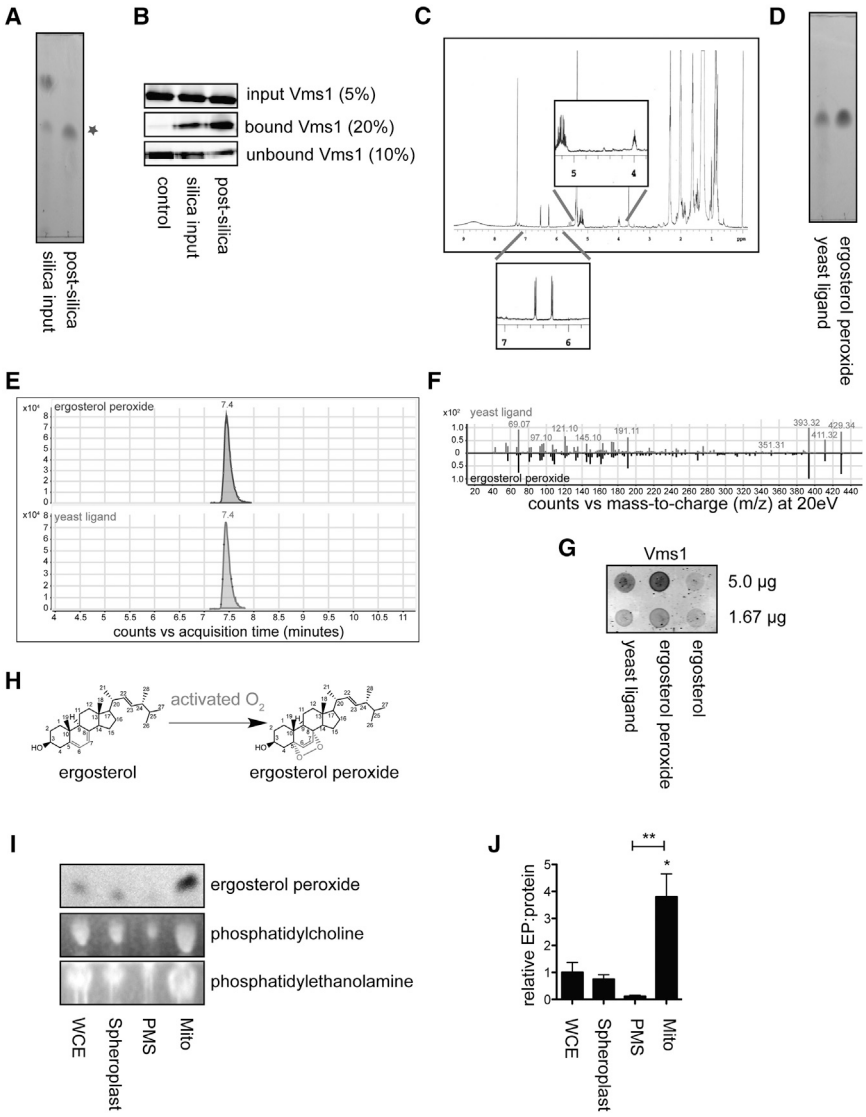

Figure 4. The $C_{28}H_{44}O_3$ Lipid Is Ergosterol Peroxide, Which Binds Vms1 Directly

(A) The $C_{28}H_{44}O_3$ species (star) was isolated from mitochondrial alkaline-resistant lipids by silica chromatography.

(B) Liposomes containing the silica chromatography input or the isolated $C_{28}H_{44}O_3$ species were prepared so that they had equivalent amounts of $C_{28}H_{44}O_3$ (lipids from approximately 1 mg mitochondria per 100 μL liposomes) and subjected to a floatation assay.

(C) ^{1}H-NMR spectrum of the isolated $C_{28}H_{44}O_3$.

(D) Comparison of the isolated $C_{28}H_{44}O_3$ species and commercial ergosterol peroxide by TLC and orcinol stain.

(E) Comparison of the isolated $C_{28}H_{44}O_3$ species and commercial ergosterol peroxide by LC-MS.

(F) Comparison of the isolated $C_{28}H_{44}O_3$ species (top) and commercial ergosterol peroxide (bottom) by MS/MS at 20 eV.

(G) Nitrocellulose membranes were spotted with equivalent amounts (5 μg [top] and 1.67 μg [bottom]) of isolated $C_{28}H_{44}O_3$ species, ergosterol peroxide, or ergosterol and assayed for binding to Vms1 by a modified immunoblot assay.

(H) The non-enzymatic oxidation of ergosterol to ergosterol peroxide.

(I) WT cells were fractionated into whole-cell extract (WCE), spheroplasts, post-mitochondrial supernatant (PMS), and mitochondria. Lipids from 2.5 mg of each fraction (by protein concentration) were analyzed by TLC and orcinol/primuline stain.

(J) Ergosterol peroxide from whole-cell extract (WCE), extract after cell-wall removal (Spheroplast), post-mitochondrial supernatant (PMS), and crude mitochondria (Mito) was quantified as the ratio of ergosterol peroxide to protein concentration over at least three experiments. Error bars, mean ± SEM. *$p \leq 0.05$; **$p \leq 0.01$.

See also Figure S2.

multiple structural analyses. As expected, the apparent binding activity toward Vms1 increased as $C_{28}H_{44}O_3$ was purified (Figures 4A and 4B), consistent with $C_{28}H_{44}O_3$ mediating Vms1 binding. We obtained a ^{1}H-NMR (nuclear magnetic resonance) spectrum of the isolated ligand (Figure 4C) and compared the peaks with published NMR spectra (Nowak et al., 2016). From this comparison, we determined that the peaks in the NMR spectra of our purified ligand were identical to those of ergosterol peroxide (EP), which has the same $C_{28}H_{44}O_3$ formula. Furthermore, our purified ligand and commercial EP possess identical retention factors by TLC (Figure 4D), identical retention times by LC-MS (Figure 4E), and equivalent tandem MS (MS/MS) spectra at multiple collision energies (Figures 4F and S2A–S2C). In combination, these data indicate that the $C_{28}H_{44}O_3$ lipid species that we isolated on the basis of its direct Vms1 binding activity is EP.

EP is an oxidized sterol, structurally differing from ergosterol only by the presence of an endoperoxide. We found that Vms1 displayed comparable binding to nitrocellulose-spotted commercial EP and the purified $C_{28}H_{44}O_3$, while displaying no affinity toward ergosterol (Figure 4G). EP is generated when highly reactive singlet oxygen and the conjugated 5,7-diene of ergosterol spontaneously cyclize, in a [4+2] Diels-Alder type cycloaddition, to generate the 5,8-endoperoxide (Figure 4H). Ergosterol is found in many membranes throughout the cell. However, we found that EP levels were specifically enriched at mitochondria relative to other cellular membranes (Figures 4I, 4J, and S4D), which is consistent with the hypothesis that EP recruits Vms1 selectively to mitochondria.

Because EP is non-enzymatically produced from ergosterol and ROS, we tested the necessity of EP for mitochondrial localization of Vms1 by eliminating these precursors. The importance of ROS was demonstrated by observing a significant reduction in Vms1^{MTD} localization to mitochondria in cells grown in anoxic conditions compared with cells grown in normoxia (Figures 5A and 5B), with no change in Vms1^{MTD}-GFP abundance (Figure S3A). Production of ergosterol, the other essential EP

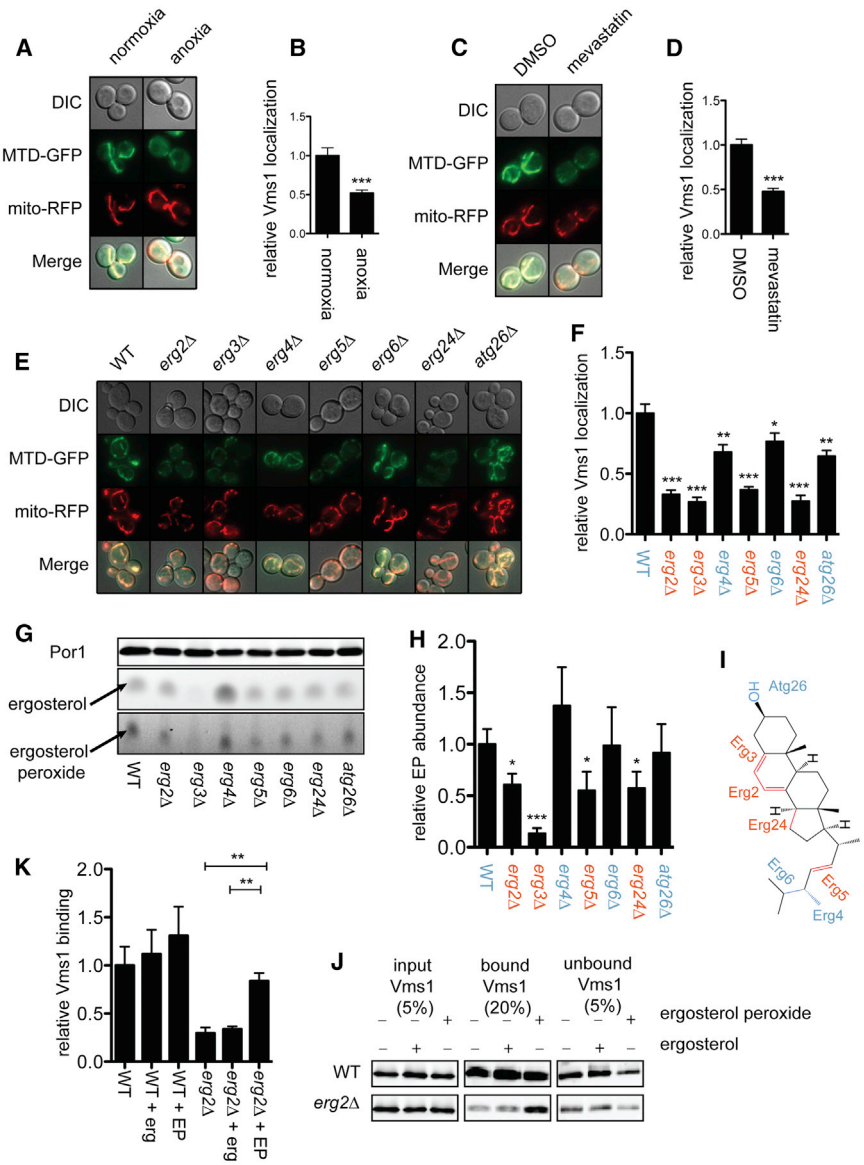

Figure 5. Ergosterol Peroxide Is Necessary for Vms1 Localization to Mitochondria

(A) WT cells expressing Vms1^{MTD}-GFP and mitochondria-targeted RFP were grown for 6 hr in anoxia or normoxia and subjected to fluorescence microscopy. Representative images are shown.

(B) The mitochondrial MTD intensity was quantified as described for 100+ cells in each condition in (A). ***$p \leq 0.001$.

(C) Cells from (A) were grown in the presence of 500 μM mevastatin or vehicle for 24 hr and subjected to fluorescence microscopy. Representative images are shown.

(D) The mitochondrial MTD intensity was quantified as described for 100+ cells in each condition in (C). ***$p \leq 0.001$.

(E) WT and the indicated mutants expressing Vms1^{MTD}-GFP and mitochondria-targeted RFP were grown to mid-log phase and subjected to fluorescence microscopy. Representative images are shown.

(F) The mitochondrial MTD intensity was quantified as described for 50+ cells in each strain in (E). Error bars, mean ± SEM. *$p \leq 0.05$; **$p \leq 0.01$; ***$p \leq 0.001$.

(G) A total of 20 μg purified mitochondria (by protein concentration) from the indicated strains was analyzed by western blot as a loading control (top). Lipids from 2 mg mitochondria from each strain were analyzed by TLC and orcinol stain.

(H) Ergosterol peroxide* from (G) was quantitated as the ratio of ergosterol peroxide* to Porin over three independent experiments. Error bars, mean ± SEM. *$p \leq 0.05$; ***$p \leq 0.001$.

(I) Structure of ergosterol indicating bonds and enzymes whose loss impairs Vms1 localization to mitochondria (red) and those that leave localization unaffected (blue).

(J) Vehicle, 3.75 μg ergosterol, or 3.75 μg ergosterol peroxide was added to mitochondrial lipids isolated from 300 μg WT or *erg2Δ* cells to make liposomes as described (STAR Methods) for use in the floatation assay.

(K) Vms1 binding to liposomes from (J) was quantified as the ratio of bound Vms1 to input Vms1 and normalized to liposomes containing no added lipids for each strain. Error bars, mean ± SEM. **$p \leq 0.01$.

See also Figure S3.

precursor, occurs through the mevalonate pathway, which is inhibited by the statin class of drugs. Statins (e.g., mevastatin) competitively inhibit HMG coenzyme A (CoA) reductase, the rate-controlling enzyme of the mevalonate pathway. We observed a significant reduction in Vms1^{MTD} localization to mitochondria upon mevastatin treatment (Figures 5C and 5D), with no effect on the steady-state abundance of Vms1^{MTD}-GFP (Figure S3B). Thus, the EP precursors, ergosterol and oxygen/ROS, are both necessary for normal Vms1^{MTD} localization to mitochondria.

Although sterol synthesis is essential for cell survival, some steps in the ergosterol biosynthetic pathway are not essential in *S. cerevisiae*. Loss of those steps leads to the synthesis of ergosterol-like species that are capable of fulfilling the essential functions of ergosterol (Böcking et al., 2000) but may be differentially capable of mediating Vms1 mitochondrial localization. To test this possibility, we measured Vms1^{MTD}-GFP localization to mitochondria (Figures 5E and 5F) and mitochondrial ergosterol and EP levels (Figures 5G and 5H) in strains lacking non-essential ergosterol biosynthetic genes. The specific "ergosterol" or "EP" species in these mutant strains are likely unique to each strain and are, therefore, indicated as ergosterol* and EP*. Vms1^{MTD} localization to mitochondria was most affected in *erg2Δ, erg3Δ*, *erg5Δ*, and *erg24Δ* mutants. Erg2 and Erg3 catalyze the formation of the 7,8 and 5,6-alkenes, respectively (Figure 5I), which constitute the 5,7-diene required for EP formation (Veen and Lang, 2005), while the desaturase Erg5 and reductase Erg24 catalyze reactions near the 5,7-diene (Figure 5I) (Veen and

Lang, 2005). In contrast, Vms1^{MTD} localization and mitochondrial EP* levels were only mildly affected in the absence of the reductase Erg4, methyltransferase Erg6, and glucosyltransferase Atg26. None of these mutants had a significant effect on Vms1^{MTD}-GFP abundance (Figure S3C). These data, therefore, indicate that Vms1^{MTD} localization to mitochondria is dependent on ergosterol biosynthesis and, particularly, on the availability of the 5,7-diene that becomes oxidized to form EP.

To determine whether EP is sufficient to promote Vms1 binding to lipid membranes, we tested the impact on Vms1 binding of introducing EP or ergosterol into liposomes prepared from mitochondrial lipids. We used mitochondrial lipids obtained from *erg2Δ* cells because this strain exhibited decreased Vms1^{MTD} localization to mitochondria and reduced levels of EP without grossly affecting the abundance of ergosterol-like sterols (Figures 5G and 5H). Exogenous addition of EP to *erg2Δ* mitochondrial lipids restored Vms1 binding, while the addition of ergosterol had no effect (Figures 5J and 5K). Taken together, these observations indicate that EP is necessary and sufficient for Vms1 binding to mitochondria and mitochondria-derived lipids.

Stress Stimulates Mitochondrial EP Abundance

Having determined that EP binds Vms1 and is necessary for Vms1 localization to mitochondria, we next sought to determine whether EP serves as a stress signal to recruit Vms1 specifically to damaged mitochondria. This idea is supported by our previous observation that Vms1 preferentially localizes to mitochondria *in vivo* that have been selectively damaged by Killer Red-generated ROS (Heo et al., 2013). Because mitochondria in the same cell that were not damaged by laser activation of the Killer Red did not show localization of Vms1, we concluded that the stress signal that promotes Vms1 translocation is confined to damaged mitochondria. To further test this hypothesis, we evaluated the *in vitro* interaction between Vms1 and mitochondria independently isolated from both stressed and unstressed cells. As predicted from the model that stressed mitochondria display enhanced Vms1 binding, we observed that mitochondria isolated from cells stressed with either rapamycin—which, among other things, induces endogenous ROS (Kissová et al., 2006)—or H_2O_2 have an increased affinity toward Vms1 *in vitro*, compared with mitochondria from unstressed cells. Conversely, Vms1 purified from stressed (rapamycin or H_2O_2) and unstressed cells exhibited identical mitochondrial binding *in vitro* (Figures 6A and 6B). This suggests that the stress-induced changes that promote Vms1 localization are localized to mitochondria.

We further demonstrated that the stress-induced change that recruits Vms1 is displayed within the mitochondrial lipid fraction by using an *in vitro* liposome-floatation binding assay. Consistent with previous results, we observed that Vms1 exhibits enhanced affinity toward liposomes prepared from mitochondrial lipids isolated from stressed cells (Figures 6C and 6D). The simplest explanation of these data is that elevated ROS causes elevated EP abundance, which recruits Vms1 to mitochondria. This model was further supported by our finding of elevated EP levels in mitochondrial lipids isolated from cells that had been treated with either rapamycin or H_2O_2 (Figures 6E and 6F).

Vms1^{LRS} and EP-Containing Membranes Compete for Vms1^{MTD} Binding

To test the hypothesis that the Vms1^{LRS} and EP-containing (EP$^+$) membranes compete for binding with the Vms1^{MTD}, we used the LRS mutant "L4A," in which four of the LRS-buried leucines are changed to alanine, which we previously showed disrupted the Vms1$^{LRS/MTD}$ interaction and promoted constitutive localization to mitochondria (Heo et al., 2013) (Figure 7A). In floatation assays, Vms1^{L4A} bound EP$^+$ liposomes substantially more strongly than Vms1^{WT} did, particularly as the amount of liposomes in the assay was decreased (Figures 7B and 7C), thereby validating that disruption of the Vms1$^{LRS/MTD}$ interaction enhances Vms1 binding to EP$^+$ liposomes.

Given that disrupting the Vms1$^{LRS/MTD}$ interaction promoted EP$^+$ membrane binding, we postulated that restricting Vms1$^{LRS/MTD}$ dissociation would reduce membrane binding. To test this idea, we engineered a Vms1 protein in which Vms1^{LRS} and Vms1^{MTD} can be tethered via chemical crosslinking and are thereby stabilized against dissociation. To crosslink Vms1 with the sulfhydryl-specific bismaleimidohexane (BMH), we introduced a single Cys in the Vms1^{LRS} and a single Cys in the Vms1^{MTD} (Vms1$^{Cys\text{-}Cys}$-HA) so that the two Cys residues would be in close proximity (Figure 7D). C387, the only reactive Cys residue in the Vms1$^{LRS/MTD}$ construct, was mutated to Ala in the Vms1$^{Cys\text{-}Cys}$ constructs. All Vms1$^{Cys\text{-}Cys}$ mutants were fully functional *in vivo* (data not shown). To monitor crosslinking, we introduced a PreScission protease site in a loop N-terminal to the Vms1^{MTD} so that migration on SDS-PAGE could distinguish the crosslinked species (Figure 7E). Importantly, protease cleavage of purified Vms1 did not alter migration on gel filtration chromatography, which indicates that the two cleaved Vms1 fragments maintained a stable association under the solution conditions used and that the structure is not grossly distorted. Cleaved Vms1^{WT} or Vms1$^{Cys\text{-}Cys}$ was incubated with DMSO or BMH crosslinker and analyzed by SDS-PAGE. Crosslinking was incomplete, but an identifiable crosslinked species appeared only in the Vms1$^{Cys\text{-}Cys}$ protein subjected to BMH (Figure 7E). Incomplete crosslinking enabled us to compare crosslinked and non-crosslinked protein within a single floatation assay. Three separate Vms1$^{Cys\text{-}Cys}$ proteins were probed for their ability to bind EP$^+$ liposomes, and all three were found to exhibit a reduced ratio of crosslinked:non-crosslinked Vms1 in liposome-bound fractions compared to input (Figures 7E and 7F). This indicates that crosslinked Vms1$^{Cys\text{-}Cys}$, in which the LRS-MTD interaction is stabilized, binds EP$^+$ membranes less efficiently than a cleaved version of the same protein in which the LRS-MTD interaction is not stabilized. These data suggest that dissociation of the Vms1$^{LRS/MTD}$ interaction is required for efficient Vms1 binding to EP$^+$ membranes.

Next, we wanted to determine the fate of the LRS when the MTD binds an EP$^+$ lipid membrane. Based on our previous results, we predicted that the LRS would dissociate from the MTD upon lipid binding. To test this model, we designed a GFP-Vms1-HA construct that contained a PreScission protease site immediately C-terminal to the LRS (Figure 7G) and followed the binding of the GFP-LRS and MTD-HA in a floatation assay. Cleavage of this Vms1 construct with PreScission protease did not alter migration on gel filtration chromatography

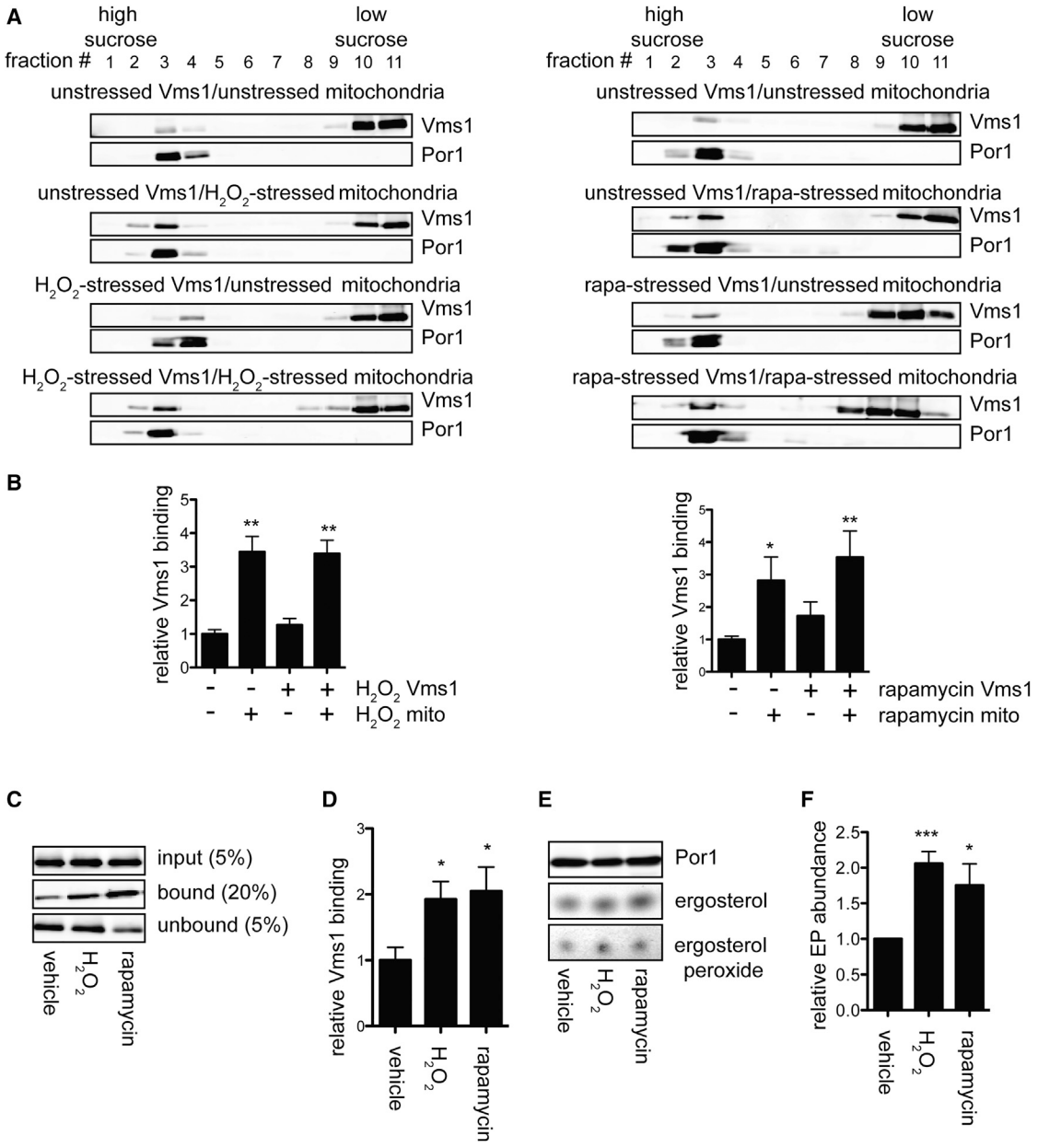

Figure 6. Increased Ergosterol Peroxide Levels in Response to Stress Correlate with Increased Vms1 Binding to Mitochondrial Lipids

(A) Purified Vms1 and mitochondria isolated from vehicle, rapamycin (rapa), or H_2O_2-treated cells were co-incubated and subjected to sucrose gradient centrifugation.

(B) Co-migration was quantitated from (A) as the ratio of Vms1 to Porin over at least 4 independent experiments. Error bars, mean ± SEM. *$p \leq 0.05$; **$p \leq 0.01$.

(C) A total of 20 μg purified mitochondria (by protein concentration) from the indicated treatments was analyzed by western blot. Lipids from 2 mg mitochondria from each strain were analyzed by TLC and orcinol stain.

(D) Ergosterol peroxide from (D) was quantitated as the ratio of ergosterol peroxide to Porin over at least three experiments. Error bars, mean ± SEM. *$p \leq 0.05$.

(E) A total of 100 μg of mitochondrial lipids isolated from cells subjected to the indicated treatments was used to make liposomes for floatation assays.

(F) Vms1 binding from (F) was quantified as the ratio of bound Vms1 to input over at least four experiments. Error bars, mean ± SEM. *$p \leq 0.05$; ***$p \leq 0.001$.

(Figures 7H and 7I), indicating that the Vms1$^{LRS/MTD}$ interaction remained intact, as observed previously. We quantified binding of the full-length construct (GFP-Vms1-HA) and the two halves of the cleaved construct (GFP-LRS/MTD-HA) to EP$^+$ liposomes in a floatation assay (Figure 7J). The difference in binding affinity was quantified as the ratio of GFP-LRS:GFP-Vms1 or MTD-HA:Vms1-HA in the bound and unbound fractions (Figure 7K). GFP-Vms1 bound more strongly than GFP-LRS, while MTD-HA bound more strongly than Vms1-HA, thereby indicating that LRS association diminishes MTD membrane-binding

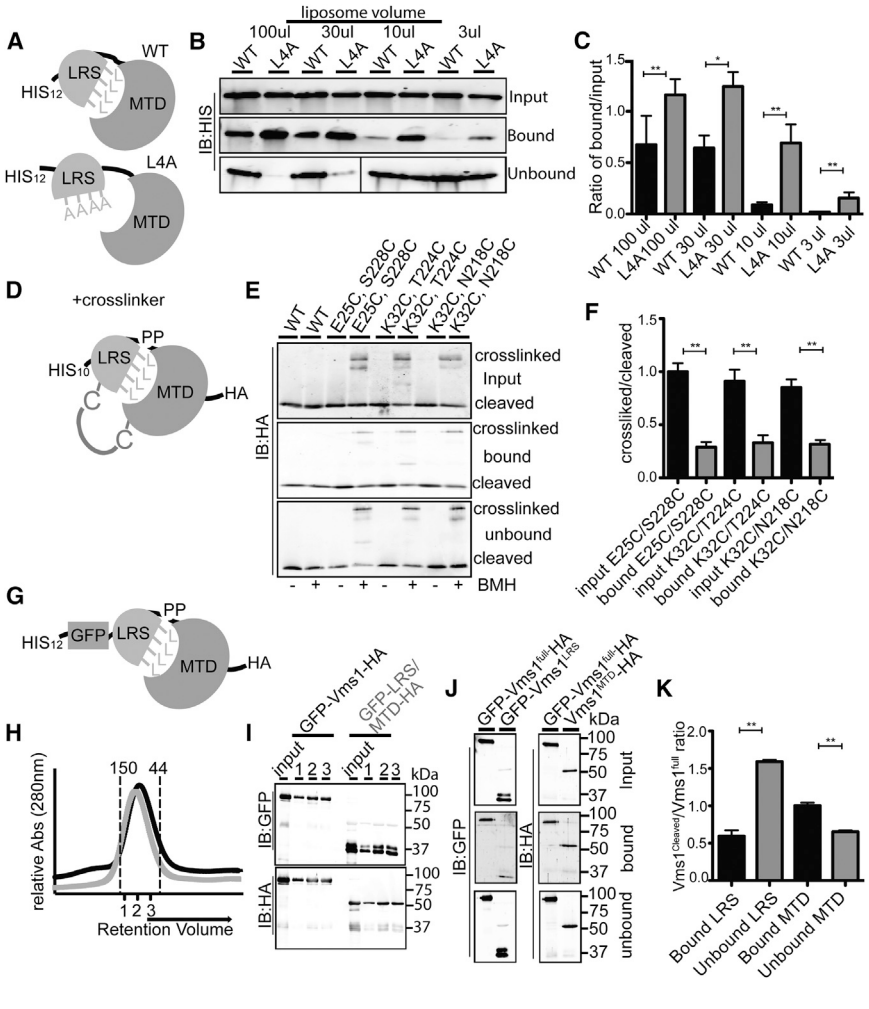

Figure 7. LRS and Lipid Compete for MTD Binding

(A) WT and L4A representations indicating that Leu-to-Ala mutations in L4A weaken the interaction with the MTD.

(B) Representative floatation assay of Vms1^{WT} or Vms1^{L4A} following incubation with liposomes (3, 10, 30, and 100 μL) containing 100 μg *erg2Δ* lipids with 1.25 μg exogenous EP per 100 μL. IB:HIS, immunoblot:HIS.

(C) Quantification of at least three floatation assay experiments from (B). Vms1 binding to liposomes was quantified as a ratio of the bound/input. Error bars, mean ± SEM. *p ≤ 0.05; **p ≤ 0.01.

(D) Cysteine residues were introduced into the Vms1^{LRS} and proximally in the Vms1^{MTD}. A PreScission protease (PP) site was introduced between the two domains to allow for observation of crosslinking efficiency on SDS-PAGE.

(E) Representative floatation assay of the indicated WT or mutant His$_{10}$-Vms1$^{1–417}$-HA constructs. Proteins with and without BMH crosslinking following incubation with PreScission protease were incubated with liposomes consisting of base lipids (DOPC, ceramide-OH, ergosterol) and 1.25 μg EP. The protein/liposome mixture was then subjected to the floatation assay.

(F) Crosslinked/cleaved protein from (E) was quantified in the input and bound fractions. Error bars, mean ± SEM. **p ≤ 0.01.

(G) His$_{12}$-GFP-Vms1^{LRS}-PP-Vms1^{MTD}-HA construct allows tracking of GFP-Vms1^{LRS} and Vms1^{MTD}-HA liposome binding within a single experiment.

(H) Size exclusion chromatogram of GFP-Vms1^{LRS}-PP-Vms1^{MTD}-HA shows equivalent elution with or without cleavage by PreScission protease. Sizing standard peaks are indicated by dashed lines. Abs, antibodies.

(I) Western blots of fractions (1–3) from (H) shows equivalent elution with or without cleavage by PreScission protease.

(J) Representative floatation assay of cleaved (GFP-Vms1^{LRS}/Vms1^{MTD}-HA) and uncleaved proteins (GFP-Vms1^{full}-HA) from (H) incubated with liposomes containing 100 μg *erg2Δ* lipids with 1.25 μg exogenous EP.

(K) Vms1^{cleaved}/Vms1^{full} ratio from experiment in (H) was quantified in the bound and unbound fractions for both GFP and HA. Error bars, mean ± SEM. **p ≤ 0.01.

See also Figure S4.

activity. Taken together, these three observations strongly support a model wherein the LRS and EP$^+$ lipid membranes compete for binding to the MTD.

Finally, we wanted to determine the effect of mutating the MTD on EP$^+$ liposome binding. Based on our model, we predicted that mutations that disrupt the LRS/MTD interface would promote membrane interaction, while mutants that maintain the LRS/MTD interaction but reduce mitochondrial localization will reduce membrane interaction. To test this model, we purified the mutants described in Figure 2 in the context of His$_{12}$-Vms1$^{1–417}$ and quantified binding to EP$^+$ liposomes (Figure S4). K194D/K196D, a mutant with reduced mitochondrial localization that maintains LRS interaction, had significantly reduced binding to liposomes (Figure S4). The other mutants maintained or increased membrane interaction, which supports the model that disrupting the LRS-MTD interaction increases EP$^+$ membrane binding *in vitro*, regardless of how the mutant behaves *in vivo*.

DISCUSSION

This study set out to answer two questions. First, we sought to discover how the Vms1^{LRS} inhibits localization of Vms1 to mitochondria. We had previously described that a highly conserved region of Vms1 (MTD) was necessary and sufficient for localization to mitochondria (Heo et al., 2013). Additionally, we showed that an LRS bound the MTD and inhibited localization to mitochondria (Heo et al., 2013). The crystal structure of Vms1 demonstrates that the LRS leucine residues, whose mutation we have shown disrupts LRS binding to the MTD and de-represses Vms1 localization to mitochondria (Heo et al., 2013), line a conserved hydrophobic groove on the MTD. Guided by the

structure, we now show that mutation of hydrophobic MTD residues at the LRS interface also disrupts LRS binding while diminishing MTD mitochondrial localization. Taken together, these structural and mutagenic data support the model that the LRS inhibits Vms1 localization to mitochondria through direct, hydrophobic interactions with the MTD and that displacement of the LRS uncovers the mitochondrial binding surface.

Second, we sought to discover the mitochondrial molecule(s) responsible for mediating $Vms1^{MTD}$ localization to mitochondria. Despite extensive effort, we failed to identify a mitochondrial protein that was important for $Vms1^{MTD}$ localization. We did, however, identify and characterize EP as a mitochondrial membrane lipid that is necessary for Vms1 mitochondrial localization. We demonstrated that Vms1 directly binds EP and that increasing EP abundance is sufficient to enhance Vms1 binding to membranes. We also found that EP is necessary for MTD localization to mitochondria *in vivo*, as we observed decreased localization when EP precursors were reduced or the ergosterol biosynthetic pathway was disrupted. Lastly, we showed that stress conditions that promote Vms1 translocation to mitochondria (rapamycin or H_2O_2) also lead to increased mitochondrial EP abundance and that the increase in EP correlates with increased Vms1 binding to lipids purified from mitochondria. Taken together, these observations indicate that EP is a necessary and sufficient receptor for Vms1 localization to mitochondria.

Having observed that EP binds the MTD to enable Vms1 localization, which is inhibited by the LRS via direct MTD binding, we wanted to understand the interplay between the LRS, EP, and their apparent competition for MTD interaction. Our biochemical experiments examined the effects of positively and negatively manipulating the LRS/MTD interaction on Vms1 binding to EP-containing (EP^+) liposomes. We showed that disrupting the MTD/LRS interaction through LRS mutation promoted binding to EP+ liposomes. Conversely, we showed that covalently tethering the LRS and MTD in order to stabilize their interaction reduced binding to EP^+ liposomes. Lastly, we showed that binding to EP^+ liposomes caused the partial dissociation of the LRS from the MTD. Altogether, these biochemical assays indicate that the LRS and EP compete for binding to the MTD and that this interplay is crucial for the regulation of Vms1 mitochondrial localization.

Overall, these data support a model wherein, under basal conditions, Vms1 is "locked" in a cytosolic conformation through intramolecular interactions between the LRS and MTD (Movie S1). The low EP abundance on the mitochondrial surface in basal conditions is insufficient to disrupt this intramolecular LRS-MTD interaction. However, mitochondrial perturbation (via rapamycin, H_2O_2, antimycin/oligomycin, paraquat, and DMNQ) elicits the production of ROS that generate mitochondrial EP through direct, non-enzymatic modification of ergosterol. This increased EP abundance subsequently competes with the LRS for $Vms1^{MTD}$ binding, thereby driving Vms1 to localize to stressed mitochondria. This mechanism would enable the rapid recruitment of the Vms1 quality control system to mitigate or repair damaged mitochondria.

Initially, it was quite surprising that EP conferred specificity for Vms1 mitochondrial localization, because its precursor, ergosterol, is more abundant in other cellular membranes (Zinser et al., 1991). In contrast, however, we found that EP is highly enriched in mitochondria. A likely explanation for the mitochondrial specificity of EP is that it is the product of non-enzymatic oxidation of ergosterol by ROS, particularly by singlet oxygen, and mitochondria are the major source of cellular ROS, which is a natural byproduct of mitochondrial respiration (Balaban et al., 2005). Moreover, ROS half-lives are typically very short (10^{-9}–10^{-5} seconds) (Forkink et al., 2010), which results in a highly localized site of action and production of EP, specifically at damaged mitochondria. An additional potential explanation for mitochondrial specificity is that EP is more rapidly degraded in non-mitochondrial membranes. Indeed, one study showed that the majority of cellular EP is rapidly converted into other oxidized forms of ergosterol by an unidentified EP isomerase (Böcking et al., 2000). This isomerase appears to be present in the secretory pathway and, therefore, might degrade EP on most other membranes but not limit the accumulation of mitochondrial EP.

The proposed model is consistent with our finding that Erg2 and Erg3 are essential for efficient Vms1 localization and binding to mitochondria. These enzymes are required for the formation of the 5,7-diene in ergosterol, which is the site of ergosterol that is modified in the conversion to EP. Moreover, *erg2Δ* and *erg3Δ* mutants exhibited decreased respiratory growth, suggesting that these mutants have defects in mitochondrial respiratory function (Smith and Parks, 1993; Steinmetz et al., 2002) that might be attributed to impaired mitochondrial Vms1 function.

In this study, we consistently observed approximately 2-fold increases of mitochondrial EP abundance and similar augmentation of Vms1 binding to mitochondria and lipids isolated from stressed (rapamycin or H_2O_2) cells. *A priori*, this relatively small increase in EP abundance might seem insufficient to confer the observed stress-responsive regulation of Vms1 translocation (Heo et al., 2010), but three issues should be considered. First, the modest increases that we observed *in vitro* are underestimates, because the mitochondrial isolation procedure itself is stressful and promotes Vms1 translocation (data not shown). Thus, we likely observed an artificially increased basal EP abundance in purified mitochondria, which would diminish the difference in Vms1 binding affinity between mitochondria from stressed and unstressed cells. Second, any membrane architecture and lipid partitioning within the MOM is lost upon extraction and reconstitution for floatation assays. Therefore, any local enrichment of EP, which would be expected based on the behavior of sterols in membranes (Bagnat et al., 2000), is lost during liposome preparation. Lastly, we suspect that Vms1 is a co-incidence detector and that elevated EP works with another signal to mediate full stress-induced Vms1 translocation. The additional signal(s) might include another specifically induced lipid or other molecule and, at a minimum, likely includes polyubiquitin, which accumulates on damaged mitochondria in the absence of Vms1 (Heo et al., 2010). For these reasons, the physiological localization of Vms1 to mitochondria in response to stress is expected be more specific and robust than suggested by the limited *in vitro* effects.

The Vms1 crystal structure revealed the direct interaction between the LRS and MTD domains. Moreover, the structure helped interpret previous mutagenesis data and design new experiments that verify that formation of the $Vms1^{LRS\text{-}MTD}$ interface

inhibits mitochondrial localization. These experiments showed that mutation of LRS residues that stabilize the interface results in enhanced mitochondrial localization. Conversely, mutation of MTD residues that stabilize the Vms1$^{LRS-MTD}$ interface reduce mitochondrial localization, indicating that these residues also participate in binding to mitochondria. The structure also raises several important questions. First, what is the disposition of the LRS when Vms1 is bound to mitochondria? Our data indicate that the LRS dissociates from the MTD but that the multiple hydrophobic LRS residues that are buried against the MTD in the cytosolic conformation are unlikely to become exposed to the cytoplasm. One attractive possibility is that the highly amphipathic LRS helix binds non-specifically to the mitochondrial membrane, as has been extensively characterized in other systems (Aberle et al., 2015). In this model, the energetic costs of displacing the hydrophobic LRS interaction—which, based on the structure, is expected to be considerable—would be offset by the recovery of hydrophobic interactions of the LRS (and, presumably, the MTD) with the membrane. Another critical question is: what is the structure of the MTD when bound to an EP^+ membrane? Because the surface of MTD covered by the LRS is large (1,205 Å^2), and because some of the MTD residues that we have shown are important for localization to mitochondria are exposed and do not make direct contact with the LRS or stabilize the MTD-LRS interaction, the interaction surface between MTD and mitochondria is likely to be considerable and/or involve a major conformational change. A structure of Vms1 bound to EP is an urgent, if challenging, goal for future studies.

We suspect that analogous lipid oxidation-based stress response mechanisms exist in higher eukaryotes. Based on the high degree of evolutionary conservation in *VMS1* across eukaryotes, particularly in the MTD, it is likely that mammalian Vms1 also interacts with an oxidized sterol to mediate mitochondrial quality control. Similarly, damaged chloroplasts produce singlet oxygen, which induces localized lipid peroxidation, subsequent ubiquitylation, and eventual removal of the organelle (Woodson, 2016; Woodson et al., 2015), which may be mediated by Vms1 or Vms1-like molecules. Therefore, we postulate that sterol oxidation might be a conserved signal of damage to engage quality control systems, including those reliant on Vms1, at organelles under oxidative stress.

STAR★METHODS

Detailed methods are provided in the online version of this paper and include the following:

- KEY RESOURCES TABLE
- CONTACT FOR REAGENT AND RESOURCE SHARING
- EXPERIMENTAL MODEL AND SUBJECT DETAILS
- METHOD DETAILS
  - Plasmids
  - Protein Expression and Purification
  - Mitochondria purification
  - Lipid isolation and alkaline hydrolysis
  - Proteinase K treatment
  - Mitochondrial co-migration assay
  - LC/MS analysis
  - Thin-layer chromatography (TLC) separation, staining, and quantification
  - Silica chromatography
  - NMR
  - Lipid blot
  - Liposome preparation
  - Liposome floatation assay
  - Microscopy
  - Site-specific crosslinking
  - Crystallization and Structure Determination
  - Co-Immunoprecipitations
- QUANTIFICATION AND STATISTICAL ANALYSIS
- DATA AND SOFTWARE AVAILABILITY

SUPPLEMENTAL INFORMATION

Supplemental Information includes four figures and one movie and can be found with this article online at https://doi.org/10.1016/j.molcel.2017.10.022.

AUTHOR CONTRIBUTIONS

J.R.N., E.K.F., C.P.H., and J.R. designed experiments and wrote the paper. E.K.F., J.R.N., and O.Z.R. conducted the experiments. H.L.S. made contributions to the X-ray crystallography. Z.L. conducted the NMR experiment. T.C.W. engineered the Cell Profiler pipeline used for microscopy quantitation.

ACKNOWLEDGMENTS

We thank Janet Iwasa for animating Movie S1. Portions of this research were performed at the Stanford Synchrotron Radiation Lightsource (SSRL). Use of the SSRL, SLAC National Accelerator Laboratory, is supported by the U.S. Department of Energy, Office of Science, Office of Basic Energy Sciences under Contract No. DE-AC02-76SF00515. The SSRL Structural Molecular Biology Program is supported by the DOE Office of Biological and Environmental Research and by the NIH, National Institute of General Medical Sciences (including P41GM103393). Mass spectrometry analysis was performed at the Metabolomics Core Facility at the University of Utah, which is supported by NIH grants 1 S10 OD016232-01, 1 S10 OD021505-01, and 1 U54 DK110858-01. This work was supported by NIH grant GM115129 (to C.P.H. and J.R.), a grant from the Nora Eccles Treadwell Foundation (to J.R. and C.P.H.), and the Howard Hughes Medical Institute (to J.R.). J.R.N. was supported by NIH grant T32GM007464. E.K.F. was supported by NIH grant T32HL007576, AHA Postdoctoral Fellowship 14POST20380216, and NIH Research Training in Hematology grant T32DK007115.

Received: August 17, 2017
Revised: October 3, 2017
Accepted: October 17, 2017
Published: November 16, 2017

REFERENCES

Aberle, D., Oetter, K.M., and Meyers, G. (2015). Lipid binding of the amphipathic helix serving as membrane anchor of pestivirus glycoprotein Erns. PLoS ONE *10*, e0135680.

Adams, P.D., Afonine, P.V., Bunkóczi, G., Chen, V.B., Davis, I.W., Echols, N., Headd, J.J., Hung, L.W., Kapral, G.J., Grosse-Kunstleve, R.W., et al. (2010). PHENIX: a comprehensive Python-based system for macromolecular structure solution. Acta Crystallogr. D Biol. Crystallogr. *66*, 213–221.

Bagnat, M., Keränen, S., Shevchenko, A., Shevchenko, A., and Simons, K. (2000). Lipid rafts function in biosynthetic delivery of proteins to the cell surface in yeast. Proc. Natl. Acad. Sci. USA *97*, 3254–3259.

Balaban, R.S., Nemoto, S., and Finkel, T. (2005). Mitochondria, oxidants, and aging. Cell *120*, 483–495.

Böcking, T., Barrow, K.D., Netting, A.G., Chilcott, T.C., Coster, H.G., and Höfer, M. (2000). Effects of singlet oxygen on membrane sterols in the yeast *Saccharomyces cerevisiae*. Eur. J. Biochem. *267*, 1607–1618.

Calvo, S.E., and Mootha, V.K. (2010). The mitochondrial proteome and human disease. Annu. Rev. Genomics Hum. Genet. *11*, 25–44.

Carpenter, A.E., Jones, T.R., Lamprecht, M.R., Clarke, C., Kang, I.H., Friman, O., Guertin, D.A., Chang, J.H., Lindquist, R.A., Moffat, J., et al. (2006). CellProfiler: image analysis software for identifying and quantifying cell phenotypes. Genome Biol. *7*, R100.

Chatzi, A., Sideris, D.P., Katrakili, N., Pozidis, C., and Tokatlidis, K. (2013). Biogenesis of yeast Mia40 - uncoupling folding from import and atypical recognition features. FEBS J. *280*, 4960–4969.

Chu, C.T., Ji, J., Dagda, R.K., Jiang, J.F., Tyurina, Y.Y., Kapralov, A.A., Tyurin, V.A., Yanamala, N., Shrivastava, I.H., Mohammadyani, D., et al. (2013). Cardiolipin externalization to the outer mitochondrial membrane acts as an elimination signal for mitophagy in neuronal cells. Nat. Cell Biol. *15*, 1197–1205.

Circu, M.L., and Aw, T.Y. (2010). Reactive oxygen species, cellular redox systems, and apoptosis. Free Radic. Biol. Med. *48*, 749–762.

Emsley, P., Lohkamp, B., Scott, W.G., and Cowtan, K. (2010). Features and development of Coot. Acta Crystallogr. D Biol. Crystallogr. *66*, 486–501.

Forkink, M., Smeitink, J.A., Brock, R., Willems, P.H., and Koopman, W.J. (2010). Detection and manipulation of mitochondrial reactive oxygen species in mammalian cells. Biochim. Biophys. Acta *1797*, 1034–1044.

Giaever, G., Chu, A.M., Ni, L., Connelly, C., Riles, L., Véronneau, S., Dow, S., Lucau-Danila, A., Anderson, K., André, B., et al. (2002). Functional profiling of the Saccharomyces cerevisiae genome. Nature *418*, 387–391.

Guan, X.L., Riezman, I., Wenk, M.R., and Riezman, H. (2010). Yeast lipid analysis and quantification by mass spectrometry. Methods Enzymol. *470*, 369–391.

Hao, H.X., Khalimonchuk, O., Schraders, M., Dephoure, N., Bayley, J.P., Kunst, H., Devilee, P., Cremers, C.W., Schiffman, J.D., Bentz, B.G., et al. (2009). SDH5, a gene required for flavination of succinate dehydrogenase, is mutated in paraganglioma. Science *325*, 1139–1142.

Heo, J.M., and Rutter, J. (2011). Ubiquitin-dependent mitochondrial protein degradation. Int. J. Biochem. Cell Biol. *43*, 1422–1426.

Heo, J.M., Livnat-Levanon, N., Taylor, E.B., Jones, K.T., Dephoure, N., Ring, J., Xie, J., Brodsky, J.L., Madeo, F., Gygi, S.P., et al. (2010). A stress-responsive system for mitochondrial protein degradation. Mol. Cell *40*, 465–480.

Heo, J.M., Nielson, J.R., Dephoure, N., Gygi, S.P., and Rutter, J. (2013). Intramolecular interactions control Vms1 translocation to damaged mitochondria. Mol. Biol. Cell *24*, 1263–1273.

Holm, L., and Rosenström, P. (2010). Dali server: conservation mapping in 3D. Nucleic Acids Res. *38*, W545–W549.

Huang, W., Choi, W., Hu, W., Mi, N., Guo, Q., Ma, M., Liu, M., Tian, Y., Lu, P., Wang, F.L., et al. (2012). Crystal structure and biochemical analyses reveal Beclin 1 as a novel membrane binding protein. Cell Res. *22*, 473–489.

Khedr, A., and Sheha, M. (2003). Quantitative thin-layer chromatographic method of analysis of azithromycin in pure and capsule forms. J. Chromatogr. Sci. *41*, 10–16.

Kissová, I., Deffieu, M., Samokhvalov, V., Velours, G., Bessoule, J.J., Manon, S., and Camougrand, N. (2006). Lipid oxidation and autophagy in yeast. Free Radic. Biol. Med. *41*, 1655–1661.

Koirala, S., Guo, Q., Kalia, R., Bui, H.T., Eckert, D.M., Frost, A., and Shaw, J.M. (2013). Interchangeable adaptors regulate mitochondrial dynamin assembly for membrane scission. Proc. Natl. Acad. Sci. USA *110*, E1342–E1351.

Kyte, J., and Doolittle, R.F. (1982). A simple method for displaying the hydropathic character of a protein. J. Mol. Biol. *157*, 105–132.

Lin, M.T., and Beal, M.F. (2006). Mitochondrial dysfunction and oxidative stress in neurodegenerative diseases. Nature *443*, 787–795.

Livnat-Levanon, N., and Glickman, M.H. (2011). Ubiquitin-proteasome system and mitochondria - reciprocity. Biochim. Biophys. Acta *1809*, 80–87.

Meisinger, C., Sommer, T., and Pfanner, N. (2000). Purification of *Saccharomcyes cerevisiae* mitochondria devoid of microsomal and cytosolic contaminations. Anal. Biochem. *287*, 339–342.

Morin, A., Eisenbraun, B., Key, J., Sanschagrin, P.C., Timony, M.A., Ottaviano, M., and Sliz, P. (2013). Collaboration gets the most out of software. eLife *2*, e01456.

Nowak, R., Drozd, M., Mendyk, E., Lemieszek, M., Krakowiak, O., Kisiel, W., Rzeski, W., and Szewczyk, K. (2016). A new method for the isolation of ergosterol and peroxyergosterol as active compounds of *Hygrophoropsis aurantiaca* and in vitro antiproliferative activity of isolated ergosterol peroxide. Molecules *21*, E946.

Otwinowski, Z., and Minor, W. (1997). Processing of X-ray diffraction data collected in oscillation mode. Methods Enzymol. *276*, 307–326.

Pettersen, E.F., Goddard, T.D., Huang, C.C., Couch, G.S., Greenblatt, D.M., Meng, E.C., and Ferrin, T.E. (2004). UCSF Chimera—a visualization system for exploratory research and analysis. J. Comput. Chem. *25*, 1605–1612.

Reiner, S., Micolod, D., Zellnig, G., and Schneiter, R. (2006). A genomewide screen reveals a role of mitochondria in anaerobic uptake of sterols in yeast. Mol. Biol. Cell *17*, 90–103.

Schuberth, C., Richly, H., Rumpf, S., and Buchberger, A. (2004). Shp1 and Ubx2 are adaptors of Cdc48 involved in ubiquitin-dependent protein degradation. EMBO Rep. *5*, 818–824.

Sherman, F. (1991). Getting started with yeast. Methods Enzymol. *194*, 3–21.

Smith, S.J., and Parks, L.W. (1993). The ERG3 gene in *Saccharomyces cerevisiae* is required for the utilization of respiratory substrates and in heme-deficient cells. Yeast *9*, 1177–1187.

Steinmetz, L.M., Scharfe, C., Deutschbauer, A.M., Mokranjac, D., Herman, Z.S., Jones, T., Chu, A.M., Giaever, G., Prokisch, H., Oefner, P.J., and Davis, R.W. (2002). Systematic screen for human disease genes in yeast. Nat. Genet. *31*, 400–404.

Studier, F.W. (2005). Protein production by auto-induction in high density shaking cultures. Protein Expr. Purif. *41*, 207–234.

Tanaka, A., Cleland, M.M., Xu, S., Narendra, D.P., Suen, D.F., Karbowski, M., and Youle, R.J. (2010). Proteasome and p97 mediate mitophagy and degradation of mitofusins induced by Parkin. J. Cell Biol. *191*, 1367–1380.

Veen, M., and Lang, C. (2005). Interactions of the ergosterol biosynthetic pathway with other lipid pathways. Biochem. Soc. Trans. *33*, 1178–1181.

Weiss, M.S. (2001). Global indicators of X-ray data quality. J. Appl. Crystallogr. *34*, 130–135.

Woodson, J.D. (2016). Chloroplast quality control—balancing energy production and stress. New Phytol. *212*, 36–41.

Woodson, J.D., Joens, M.S., Sinson, A.B., Gilkerson, J., Salomé, P.A., Weigel, D., Fitzpatrick, J.A., and Chory, J. (2015). Ubiquitin facilitates a quality-control pathway that removes damaged chloroplasts. Science *350*, 450–454.

Ye, Y., Meyer, H.H., and Rapoport, T.A. (2003). Function of the p97-Ufd1-Npl4 complex in retrotranslocation from the ER to the cytosol: dual recognition of nonubiquitinated polypeptide segments and polyubiquitin chains. J. Cell Biol. *162*, 71–84.

Yoshii, S.R., Kishi, C., Ishihara, N., and Mizushima, N. (2011). Parkin mediates proteasome-dependent protein degradation and rupture of the outer mitochondrial membrane. J. Biol. Chem. *286*, 19630–19640.

Zinser, E., Sperka-Gottlieb, C.D., Fasch, E.V., Kohlwein, S.D., Paltauf, F., and Daum, G. (1991). Phospholipid synthesis and lipid composition of subcellular membranes in the unicellular eukaryote *Saccharomyces cerevisiae*. J. Bacteriol. *173*, 2026–2034.

Zorov, D.B., Juhaszova, M., and Sollott, S.J. (2014). Mitochondrial reactive oxygen species (ROS) and ROS-induced ROS release. Physiol. Rev. *94*, 909–950.

STAR★METHODS

KEY RESOURCES TABLE

REAGENT or RESOURCE	SOURCE	IDENTIFIER
Antibodies		
Mouse monoclonal anti-His	Clontech	Cat#631212
Mouse monoclonal anti-HA	BioLegend	Cat#MMS-101P-500
Rabbit polyclonal anti-HA	BioLegend	Cat#PRB-101C-200
Mouse monoclonal anti-Porin	Abcam	Cat#110326
Rabbit anti-HSP70	Dr. Kostas Tokatlidis: (Chatzi et al., 2013)	N/A
Rabbit polyclonal anti-GFP	Sigma-Aldrich	Cat#G1544
Rabbit polyclonal anti-Fzo1	(Heo et al., 2010)	N/A
Rabbit anti-Mia40	Dr. Kostas Tokatlidis: (Chatzi et al., 2013)	N/A
Rabbit polyclonal anti-Sdh1	21st Century Biochemicals	#Pr1852a
Rabbit polyclonal anti-Sdh2	21st Century Biochemicals	#Pr1633
Rabbit anti-Tom22	Dr. Kostas Tokatlidis: (Chatzi et al., 2013)	N/A
Mouse monoclonal anti-Pgk1	Abcam	Cat#AB113687
Chemicals, Peptides, and Recombinant Proteins		
Bismaleimidohexane (crosslinker)	Thermo Fisher	Cat#22330
Orcinol	Sigma Aldrich	Cat#447420
Rapamycin	LC Laboratory	Cat#R-5000
Hydrogen peroxide	Millipore	Cat#386790
Proteinase-K	New England BioLabs	Cat#P8107S
Anti-HA magnetic beads	Thermo Scientific	Cat#88836
Deposited Data		
Yeast Vms1 (1-417) crystal structure	This study	PDB: 5WHG
Experimental Models: Organisms/Strains		
JRY762: *MATa leu2-3,112 trp1-1 can1-100 ura3-1 ade2-1 his3-11,15*	(Heo et al., 2010)	N/A
JRY764: *MATa leu2-3,112 trp1-1 can1-100 ura3-1 ade2-1 his3-11,15 vms1Δ::*KanMX	(Heo et al., 2010)	N/A
JRY1734: *BCY213 MATa pep4Δ::HIS3 prb1Δ::LEU2 bar1Δ::HISG lys2::GAL1/10-GAL4 can1 ade2 trp1 ura3 his3 leu2-3,112*	Brad Cairns Lab	N/A
JRY2509: *MATa his3Δ1 leu2Δ0 met15Δ0 ura3Δ0*	This study	N/A
JRY3483: *erg2Δ MATa his3Δ1 leu2Δ0 met15Δ0 ura3Δ0 erg2::kanMX*	(Giaever et al., 2002)	N/A
JRY3484: *erg3Δ MATa his3Δ1 leu2Δ0 met15Δ0 ura3Δ0 erg3::kanMX*	(Giaever et al., 2002)	N/A
JRY3485: *erg4Δ MATa his3Δ1 leu2Δ0 met15Δ0 ura3Δ0 erg4::kanMX*	(Giaever et al., 2002)	N/A
JRY3486: *erg5Δ MATa his3Δ1 leu2Δ0 met15Δ0 ura3Δ0 erg5::kanMX*	(Giaever et al., 2002)	N/A
JRY3487: *erg6Δ MATa his3Δ1 leu2Δ0 met15Δ0 ura3Δ0 erg6::kanMX*	(Giaever et al., 2002)	N/A
JRY3488: *erg24Δ MATa his3Δ1 leu2Δ0 met15Δ0 ura3Δ0 erg24::kanMX*	(Giaever et al., 2002)	N/A

(*Continued on next page*)

Continued

REAGENT or RESOURCE	SOURCE	IDENTIFIER
JRY3489 *atg26Δ MATa his3Δ1 leu2Δ0 met15Δ0 ura3Δ0 atg26::kanMX*	(Giaever et al., 2002)	N/A
Recombinant DNA		
pJR 13811 pGST parallel, GST-TEV-Vms1(Δ38-69, 1-417)	This study	N/A
pJR192, URA3, cen (EV)	Stratagene	pRS416
pJR132011A URA3, cen, P_{VMS1}-VMS1^{MTD}(182-147)-GFP	This study	N/A
pJR13819 URA3, cen, P_{VMS1}-VMS1^{MTD}(182-147, Y190D)-GFP	This study	N/A
pJR13816 URA3, cen, P_{VMS1}-VMS1^{MTD}(182-147, I191D)-GFP	This study	N/A
pJR13812 URA3, cen, P_{VMS1}-VMS1^{MTD}(182-147, F193D)-GFP	This study	N/A
pJR13840 URA3, cen, P_{VMS1}-VMS1^{MTD}(182-147, K194D, K194D)-GFP	This study	N/A
pJR13836 URA3, cen, P_{VMS1}-VMS1^{MTD}(182-147, Y197D)-GFP	This study	N/A
pJR13813 URA3, cen, P_{VMS1}-VMS1^{MTD}(182-147, I206D)-GFP	This study	N/A
pJR13839 URA3, cen, P_{VMS1}-VMS1^{MTD}(182-147, Y207D)-GFP	This study	N/A
pJR13817 URA3, cen, P_{VMS1}-VMS1^{MTD}(182-147, F246D)-GFP	This study	N/A
pJR13838 URA3, cen, P_{VMS1}-VMS1^{MTD}(182-147, H253E,Q254E, R255E)-GFP	This study	N/A
pJR13837 URA3, cen, P_{VMS1}-VMS1^{MTD}(182-147, Y285D, T286D)-GFP	This study	N/A
pJR13835 URA3, cen, P_{VMS1}-VMS1^{MTD}(182-147, L277D, H279A)-GFP	This study	N/A
pJR13815 URA3, cen, P_{VMS1}-VMS1^{MTD}(182-147, F372D)-GFP	This study	N/A
pJR13814 URA3, cen, P_{VMS1}-VMS1^{MTD}(182-147, Y391D)-GFP	This study	N/A
pJR13841 URA3, cen, P_{VMS1}-VMS1^{MTD}(182-147, L392D)-GFP	This study	N/A
pJR10759A, P_{VMS1}-VMS1(1-182)-6HIS-2HA	(Heo et al., 2013)	N/A
pJR13842, 10HIS-VMS1(1-182-PP-417)-HA	This study	N/A
pJR13843, 10HIS-VMS1(1-182-PP-417, C387A, E25C, S228C)-HA	This study	N/A
pJR13844, 10HIS-VMS1(1-182-PP-417, C387A, K32C, T224C)-HA	This study	N/A
pJR13845, 10HIS-VMS1(1-182-PP-417, C387A, K32C, N218C)-HA	This study	N/A
pJR10755B URA3, 2μ, p_{GAL1}-12HIS-VMS1(1-417)	This study	N/A
pJR10756A URA3, 2μ, p_{GAL1}-12HIS-VMS1(L4A, 1-417)	This study	N/A
pJR 13820 URA3, 2μ, p_{GAL1}-12HIS-GFP-VMS1-1-37-PP-417-HA)	This study	N/A
pJR132011A, URA3, cen, P_{VMS1}-VMS1^{MTD}(182-147)-GFP	This study	N/A
Software and Algorithms		
Zen	Zeiss	https://www.zeiss.com/microscopy/us/products/microscope-software/zen.html
Phenix	(Adams et al., 2010)	N/A
Coot	(Emsley et al., 2010)	N/A

(*Continued on next page*)

Continued

REAGENT or RESOURCE	SOURCE	IDENTIFIER
Cell Profiler	(Carpenter et al., 2006)	http://cellprofiler.org
Chimera	(Pettersen et al., 2004)	N/A
HKL2000	(Otwinowski and Minor, 1997)	N/A
ImageJ	NIH	https://imagej.nih.gov/ij/

CONTACT FOR REAGENT AND RESOURCE SHARING

Further information and requests for reagents may be directed to and will be fulfilled by the Lead Contact, Jared Rutter (rutter@biochem.utah.edu).

EXPERIMENTAL MODEL AND SUBJECT DETAILS

Saccharomyces cerevisiae strain JRY2509 (*MATa his3 leu2 ura3 met15*) was used as the WT strain. Deletion mutant strains were taken from the *Saccharomyces* Genome Deletion Project (Giaever et al., 2002). Yeast were transformed by the lithium acetate method, and grown at 30°C in SD medium (0.67% yeast nitrogen base, 2% glucose) with amino acids unless otherwise indicated (Sherman, 1991). To test the effect of stress on Vms1-mitochondria co-migration, WT cells transformed with empty vector were grown to mid-log phase in SD-Ura medium and treated with one of the following prior to harvesting: 200 ng/mL rapamycin (LC Laboratory #r-5000) for 2.5 hours or 3 mM H_2O_2 (Millipore #386790) for 90 minutes.

METHOD DETAILS

Plasmids

A plasmid (pJR132011A) expressing C-terminally GFP-tagged Vms1^{MTD} was generated by PCR amplifying the *VMS1* coding region from nucleotide 544 to 1251 and the *VMS1* promoter from 335 nucleotides upstream to the *VMS1* start codon from genomic DNA and ligating them in frame into a pRS416-based vector containing a GFP tag (pJR1415A). Mitochondria were identified with a plasmid (pJR9509B) encoding RFP targeted to mitochondria as described previously (Heo et al., 2010). Details of expression constructs are given in key resources table. All mutations and deletions were introduced via sewing PCR.

Protein Expression and Purification

The Vms1$^{1\text{-}417,\ \Delta 38\text{-}69}$ construct was expressed in BL21(DE3) codon+(RIL) *E. coli* cells (Stratagene #230245) in autoinduction media ZYP-5052 (Studier, 2005). Cultures were grown in baffled flasks at 37°C to an optical density 600 (OD600) of ~0.5 and transferred to 19°C for ~18 hours. Cultures were harvested via centrifugation and pellets were frozen at −80°C. Pellets were resuspended in ice cold lysis buffer (20 mM Tris pH 8.0, 300 mM NaCl, 5% glycerol, 1 mM DTT) supplemented with protease inhibitors (aprotinin, leupeptin, pepstatin A, and PMSF) (Sigma). Resupended cells were treated with 100 ug/ml lysozyme (Gold Biotechnology #L-040-100) and DNase (Gold Biotechnology #9003-98-9) for 30 minutes and then subjected to sonication. Sonicated lysates were clarified via centrifugation.

Recombinant Vms1 was purified via three chromatographic steps at 4°C. Purification was monitored by SDS-PAGE. Clarified lysate was incubated with Glutathione Sepharose resin (EMD Biosciences #70541-4) for ~3 hours, washed with 3 × 10 column volumes (CV) of lysis buffer, and incubated with 10 CV of low salt lysis buffer (100 mM NaCl) containing TEV protease (0.005 mg/ml) overnight. Protein cleaved off of the GST resin was loaded on a Hi-Trap Q HP column (GE Healthcare #17-1154-01), washed with 10 cv of low salt lysis buffer, and eluted with a 0-500mM NaCl gradient over 15 cv. Q fractions containing Vms1 were concentrated and run on a Superdex 200 (GE Healthcare) gel filtration column equilibrated in low salt lysis buffer. For purification of the selenomethionine-substituted protein, 3 mM DTT was used instead of 1 mM DTT.

For the His_{10}-Vms1$^{Cys\text{-}Cys}$ proteins, constructs were expressed and lysed as described above, except that DTT was not included in the lysis buffer. Clarified lysates were added to Ni-NTA resin (QIAGEN #30250) for 1 hour, washed with 10 CV of lysis buffer, 10 cv of lysis buffer with 40 mM imidazole, and eluted with lysis buffer with 250 mM imidazole. Eluted protein was dialyzed into lysis buffer to remove the imidazole, concentrated, and run on a Superdex 200 as described above.

For the His_{12} tagged proteins, constructs were transformed into JRY1734 (pep4::HIS3 prb1::LEU2 bar1::HISG lys2::GAL1/10-GAL4) and grown in synthetic media lacking Uracil with 3% glycerol and 2% ethanol. When the OD 600 reached ~0.5, 0.5% galactose was added to the cultures and incubated for 6 hours. Cells were harvested, washed with sterile H2O, and flash frozen. Cells were lysed using a pulverizer (SPEX SamplePrep 6870) and the lysed powder was thoroughly resuspended in the above lysis buffer. The resuspended lysate was clarified via centrifugation, and purified as described for Vms1$^{Cys\text{-}Cys}$.

Mitochondria purification

Cells were exposed to the indicated conditions and harvested in mid-log phase. Mitochondria were then purified by sucrose gradient ultracentrifugation as previously described (Hao et al., 2009).

Lipid isolation and alkaline hydrolysis

Lipids were isolated from mitochondria, post-mitochondrial supernatant (PMS), or whole cell extract (WCE) using a modified Folch extraction. Pelleted mitochondria (1-5mg as measured by protein concentration) were resuspended in 500 μL of PBS (GIBCO). 500 μL of methanol (Sigma) and 1 mL of chloroform (Fisher Scientific) were added to 500 μL of WCE, PMS, or resuspended mitochondria and vortexed at high speed for 10 minutes. The resulting mixture was centrifuged for two minutes at 1000x*g*. The lower organic phase was transferred to a new tube and the remaining aqueous phase was extracted with chloroform two additional times. The pooled organic extracts were washed two times with water, and the washed organic extract evaporated by SpeedVac (Savant) to yield a lipid film. This lipid film was analyzed as a total lipid fraction or subjected to NaOH hydrolysis as previously described (Guan et al., 2010) to create an alkaline-resistant lipid fraction enriched for sterols, and sphingolipids.

Proteinase K treatment

Purified mitochondria were resuspended in SEM buffer (250 mM sucrose, 1 mM EDTA, 10 mM MOPS pH 7.2) to a concentration of 5 mg/mL. 1 μL of Proteinase K (New England BioLabs #P8107S) was added for every 50 μg of mitochondria, the mixture was quickly mixed, and then incubated on ice for 30 minutes. 1 μL of 25 mg/mL PMSF (in isopropanol) was added for every 50 μg of mitochondria, and the resulting mixture was centrifuged at 3000x*g* for 5 minutes after which the supernatant was discarded. The pellet was washed with 250 μL SEM buffer, centrifuged at 3000x*g* for 5 minutes, and the supernatant discarded. To test the efficiency of protein cleavage at the MOM, untreated and proteinase K-treated mitochondria were subjected to SDS-PAGE and western blot for Fzo1 (Dr. Janet Shaw), Tom22 (Dr. Kostas Tokatlidis), Por1 (Abcam #110326), Mia40 (Dr. Kostas Tokatlidis), Sdh1 (21st Century Biochemicals #Pr1852a), and Sdh2 (21st Century Biochemicals #Pr1633).

Mitochondrial co-migration assay

100μg of purified mitochondria were incubated with 2.5 μg of purified recombinant His_{10}-$Vms1^{1-417}$-HA in 300 μL of SEM buffer for 1 hour at 4°C. 30 μL was taken as an input control and the remaining mixture was loaded on a step-sucrose gradient (60%, 32%, 23%, 15% sucrose in MOPS buffer) and mitochondria-bound Vms1 was separated from unbound Vms1 by high speed ultracentrifugation as previously described (Meisinger et al., 2000). After centrifugation, fractions were collected, TCA precipitated, and subjected to SDS-PAGE and western blot with α-His_6 (Clontech #631212) and α-Por1 (Abcam #110326) antibodies.

LC/MS analysis

Samples were resuspended in 25 μL of isopropyl alcohol (IPA):water:acetonitrile (ACN) (72:16:12) in 10 mM ammonium formate and 0.1% formic acid, centrifuged for 5 min at 15,000 g, and the supernatant transferred to a LC/MS vial with insert. Lipid extracts were separated on an Acquity UPLC Charged Surface Hybrid C18 1.7 μm 2.1 × 100 mm column maintained at 60°C connected to an Agilent HiP 1290 Sampler, Agilent 1290 Infinity pump, equipped with an Agilent 1290 Flex Cube and Agilent 6520 Accurate Mass Quadrupole time-of-flight dual electrospray ionization mass spectrometer. The source gas temperature was set to 350°C, with a gas flow of 11.1 L/min and a nebulizer pressure of 24 psig. Capillary voltage was 5000 V, fragmentor voltage 250 V, skimmer voltage 74.4 V, and Octopole RF peak voltage 750 V. Reference masses (m/z 121.0509 and 922.0098) were infused with nebulizer pressure at 2 psig and acquired with the scan range between m/z 100 – 1700 in positive mode. Mobile phase A comprised ACN:water (60:40 v/v) in 10 mM ammonium formate and 0.1% formic acid, and mobile phase B comprised IPA:water (90:10 v/v) in 10 mM ammonium formate and 0.1% formic acid. The chromatography gradient started at 15% mobile phase B, increased to 30% B over 4 min, increased to 52% B from 4-5 min, increased to 82% B from 5-22 min, increased to 95% B from 22-23 min, and then increased to 99% B from 23-27 min. From 27-38 min it was held at 99%B, then decreased to 15% B from 38-38.2 min, and was held at that level from 38.2-44 min. The flow rate was 0.3 mL/min throughout. The injection volume was 20 μL for fractionation experiments and 3μL for analytical experiments. For fractionation experiments, we used an in-line splitter, to divert post-column flow at a 10:1 ratio to collect 1 min fractions (0.3 mL per fraction), with the 1 part used for mass spectrometry analysis and the other 10 parts for liposome formation. Tandem mass spectrometry was conducted with the same LC gradient and source conditions, but without fraction collection, in the negative mode using collision energies of 10 eV, 20 eV and 40 eV.

Thin-layer chromatography (TLC) separation, staining, and quantification

Lipids were dissolved in 1:1 chloroform:methanol and spotted on to TLC plates (EMD Millipore #1.05554.0001). The TLC was resolved in a 40:1 chloroform:methanol solvent system. Lipids were extracted from TLC plates by vortexing the strip of TLC plate in a 1:1 chloroform:methanol mixture for 10 minutes. The TLC strip was removed and the mixture was centrifuged for two minutes at high speed to pellet the loose silica. The supernatant was transferred to a fresh tube and the resulting organic solution was evaporated by SpeedVac (Savant) to produce a lipid film. TLC plates were stained with an orcinol solution. 200 mg of orcinol (Sigma) were dissolved in 11.4 mL of H_2SO_4 and brought up to 100 mL with water. Resolved TLC plates were submerged briefly in the orcinol solution, left to air dry for five minutes, and then heated on a hot plate at ~95°C until bands appeared. TLC has been repeatedly used to

quantify abundance (Khedr and Sheha, 2003). For EP quantification, we ran a dilution series of commercial EP and quantified each standard spot on the TLC using ImageJ. Using these values, we generated standard curves with R^2 values $\geq$ 0.97, suggesting that dilutions of the EP standards can be accurately quantified using TLC. We then quantified our unknown samples at a dilution where the EP band was in the linear range of our standard curve.

Silica chromatography

Starting at the base of the column, a classic preparative chromatography column (with solvent reservoir) was prepared with a glass wool plug, washed sand (Fisher Scientific), silica gel (VWR International #SX0143U-1) at a ratio of 50:1 silica mass:sample mass that had been suspended in hexane (Sigma), and another layer of washed sand on top. The hexane was drained from the column and the lipid mixture, resuspended in hexane, was loaded slowly on to the column and allowed to migrate through the sand into the silica gel layer. Lipids were eluted with the following solvent system: 1 column volume hexane (Sigma), 2 column volumes dichloromethane (Fisher Scientific), 2 column volumes of 1:1 dichloromethane:chloroform (Fisher Scientific), and then chloroform until the desired $C_{28}H_{44}O_3$ had completely eluted as monitored by TLC.

NMR

1-H NMR spectra were acquired with $CDCl_3$ (deutered chloroform) as the solvent on a Varian Inova 500 MHz NMR spectrometer in the University of Utah NMR Core Facility.

Lipid blot

1 μL of a lipid solution, containing lipids purified from yeast, EP (Chemfaces #CFN98035), or ergosterol (Fisher Scientific #AC11781), in 100% chloroform was spotted on to nitrocellulose membrane (Fisher Scientific #10600002). The membrane was blocked with 3% fatty-acid free BSA (Sigma #A6003) in TBS (25 mM Tris, 150 mM NaCl, pH 7.5) for one hour at room temperature. The blocking solution was replaced with a 1 μg/mL solution of His_{12}-$Vms1^{1\text{-}417}$-HA in TBS with 3% fatty-acid free BSA and incubated overnight at 4°C. The membrane was then subjected to standard western blot techniques with 1° and 2° antibody incubation in TBS with 3% fatty-acid free BSA to visualize protein-lipid binding.

Liposome preparation

A control lipid solution was prepared by mixing 0.82 molar equivalents of DOPC (Avanti #850375P) and 0.18 molar equivalents of cholesterol (Avanti #700000P) in a glass vial. Additional lipids were added to the control liposome solution where indicated. Solvent was evaporated by gentle vortexing under a steady stream of argon gas to make a lipid film around the walls of the vial. These films were dried under vacuum for one hour at −52°C. The lipid film was then resolubilized in hexane (Sigma) and subsequently evaporated under a gentle stream of argon while vortexing, followed by a second round of vacuum-drying for three to four hours at −52°C. Lipid films were then hydrated with TBS to produce a 1mg lipid/mL buffer mixture. This mixture was rotated overnight at 4°C and extruded through 1.0 μM membranes (Fisher Scientific #05-71-5120) to produce a semi-homogeneous liposome population. Aliquots were stored at −80°C. Liposomes prepared from total mitochondrial lipids were prepared without the addition of DOPC and cholesterol. Total mitochondrial lipids isolated from the indicated strains and additional lipids, if indicated, were mixed and dissolved in chloroform. Liposomes were prepared from this lipid solution as described above.

Liposome floatation assay

100 μL of liposomes were incubated with 2.5 μg of purified Vms1 protein at 4°C for one hour. 10 μL of the mixture was taken as an input control and mixed 1:1 with 4X laemmeli buffer (40% glycerol, 250 mM Tris-HCl pH 6.8, 8%SDS, 0.04% bromophenol blue, 0.1M DTT). 300 μL of 2M sucrose in TBS was added to the liposome-protein mixture and mixed well. A step-sucrose gradient was then created by gently loading 300 μL of 1M sucrose in TBS on top of the liposome mixture, followed by 300 μL of 0.5 M sucrose in TBS, and finally 75 μL of TBS. This was spun for 30 minutes in a Beckman Optima-Max table-top ultracentrifuge at 55,000 rpm allowing the liposomes to float to the top of the gradient, thereby separating unbound protein from liposome-bound protein (Koirala et al., 2013). 150 μL was taken from the top (bound Vms1) and bottom (unbound Vms1) of the sucrose gradient and analyzed by SDS-PAGE and western blot with α-His_6 antibody (Clontech #631212).

Microscopy

The WT (JRY2509) or mutant strains were transformed with a plasmid expressing $Vms1^{MTD}$-GFP (or point mutants) under the native *VMS1* promoter and a plasmid expressing mitochondria-targeted RFP. The cells were grown to mid-log phase and then imaged using a Zeiss Axioplan 2 Imaging microscope (Carl Zeiss). To test the effect of statin-treatment on $Vms1^{MTD}$ localization, WT cells transformed with a plasmid expressing $Vms1^{MTD}$-GFP under the native *VMS1* promoter and a plasmid expressing mitochondria-targeted RFP were inoculated, back-diluted, and grown in media containing vehicle or 500 μM mevastatin (Santa Cruz Biotech #SC-200853A) for 24 hours prior to imaging. To test the dependence of Vms1 lipid receptor production on the presence of oxygen, WT (JRY2509) cells were transformed with a plasmid expressing $Vms1^{MTD}$-GFP under the native *VMS1* promoter and a plasmid expressing mitochondria-targeted RFP. After reaching mid-log phase, these cells were grown for 6 hours either in anoxia or normoxia with

supplemented ergosterol (20 μg/mL) and fatty acids (5 mg/mL Tween 80) (Reiner et al., 2006). After the 6-hour treatment cells were imaged as described above.

Site-specific crosslinking

Purified $Vms1^{Cys\text{-}Cys}$ proteins were incubated with PreScission protease (0.01 mg/ml) overnight and run on SDS-PAGE to monitor cleavage. Cleaved protein was desalted into 20 mM Tris pH 8.0, 300 mM NaCl, 5% glycerol to remove any reducing agent. 1 μl of either DMSO or 2 mM bismaleimidohexane (BMH, ThermoFisher #22330) were added 100 μl of 0.5 mg/ml protein and incubated on ice for 2 hours. Crosslinked was quenched by adding 3 mM DTT to the reaction.

Crystallization and Structure Determination

Gel filtration fractions containing Vms1 were concentrated to ~10 mg/ml for crystallization trials. All crystals were grown in sitting drops of 1:1 protein:reservoir at 13°C. Vms1 was initially crystallized against a reservoir of 20% PEG MME 2000, 100 mM Tris pH 8.5, and 0.2 M TMAO (Index screen F2, Hampton Research #HR2-144). Optimized crystals were obtained by screening around the initial reservoir conditions (22%–24% PEG was ideal) combined with streak seeding after ~1 day.

Crystals were briefly immersed in reservoir solution with 20% glycerol and plunged into liquid nitrogen prior to data collection. Diffraction data were collected on SSRL beamline 11-1 at a wavelength of 0.97925 Å (selenomethionine inflection) with a Pilatus 6M detector, and were processed with HKL2000 (Otwinowski and Minor, 1997). The structure was determined by the SAD method and refined using PHENIX (Adams et al., 2010). The model was built using COOT (Emsley et al., 2010). Figures of molecular structures were made in Chimera (Pettersen et al., 2004). SBGrid was used throughout the structure determination (Morin et al., 2013). See Table 1 for crystallography statistics.

Co-Immunoprecipitations

p^{VMS1}-$VMS1^{1\text{-}182}$-HIS_6-HA was co-expressed with p^{VMS1}-$Vms1^{182\text{-}417}$-GFP in JRY764 (*vms1Δ*). ~50 OD were harvested and resuspended in IP buffer (20 mM Tris pH 7.4, 50 mM NaCl, 0.2% Triton X-100), vortexed, clarified via centrifugation, and added to anti-HA magnetic beads (Thermo scientific #88836). After 4 hours of incubation, beads were pelleted at 2K G and washed 4X with 1ml of IP buffer. Proteins were eluted with 50 ul of 2X laemmli buffer (20% glycerol, 125 mM Tris-HCl pH 6.8, 4% SDS, 0.02% bromophenol blue).

QUANTIFICATION AND STATISTICAL ANALYSIS

All western blots were quantitated using ImageJ 1.50i software. Microscopy was quantified as the mean GFP intensity ($Vms1^{MTD}$-GFP) in pixels containing RFP signal (mitochondria) using Cell Profiler (Carpenter et al., 2006). All statistics are derived from the comparison of the mean ± standard error of the mean in each experimental condition to the WT or control sample utilizing an unpaired t test, unless specifically indicated otherwise. * $p \leq 0.05$, ** $p \leq 0.01$, ***$p \leq 0.001$.

DATA AND SOFTWARE AVAILABILITY

The accession number for coordinates and structure factor amplitudes reported in this paper is PDB: 5WHG.